A SERVO CONTROLLED DYNAMIC LOAD MICROBALANCE

By

HARVARD LYNN TOMLINSON

Bachelor of Science

Oklahoma State University

Stillwater, Oklahoma

1963

Submitted to the faculty of the Graduate School of
the Oklahoma State University
in partial fulfillment of the requirements
for the degree of
MASTER OF SCIENCE
August, 1964

A SERVO CONTROLLED DYNAMIC LOAD MICROBALANCE

Thesis Approved:

Paul G. McCollum
Thesis Adviser

Daniel Sisler

Dean of the Graduate School

ACKNOWLEDGMENTS

The author wishes to express his appreciation to Mr. Paul McCollum and Dr. Robert D. Freeman for their advice and guidance in planning this study. Special thanks to Dr. Freeman who made available the apparatus upon which this thesis is based. Appreciation and gratitude also go to Judy Humes and Betty Bellis who performed invaluable assistance in the final preparation of this thesis. The author also wishes to express his gratitude to his wife for her patience and encouragement. Finally, the author wishes to express sincere thanks to the Physics Machine Shop, in particular Heinz Hall, for their excellent work in fabricating the entire microbalance system.

TABLE OF CONTENTS

TABLE OF CONTENTS
(Continued)

LIST OF TABLES

LIST OF FIGURES

LIST OF FIGURES
(Continued)

CHAPTER I

THE PROBLEM

Statement of the Problem

In physical chemistry research the use of continuous null or dynamic microbalances is quite common as a means of measuring weights or weight losses in the microgram region. This is particularly true in the field of high temperature physical chemistry where the properties of the vaporization of metals are studied in some detail. The writer has investigated the control system of such a balance and has analyzed its characteristics and behavior. This thesis is the result of these studies.

Uniqueness of the Problem

In recent years, the development of highly specialized and sophisticated metals and other materials has placed a great burden on the instrumentation field. The ever increasing requirement for greater accuracy in measurement of quantity, purity, structure, etc., of materials forces the same requirement for accuracy on the methods of measurement. For example, in the study of metals at high temperatures, the collection of experimental data such as vapor pressure and weight loss of vaporizing metals requires a balance with a sensitivity in the microgram region. The development of such a microbalance requires the solving of a host of control design problems.

After making an intensive search, the writer found a deficiency in the literature in analyses of control systems employed in automatic microbalances. Generally, detail is confined to the vacuum techniques and the measuring techniques. Thus, the writer set as his task the study and report of various aspects of automatic control of a particular type of microbalance--a continuous null microbalance. This system employs a closed-loop control system and has the unique property of controlling very small process changes. In other words, the control system is required to make continuous adjustment for extremely small weight changes.

CHAPTER II

TYPES OF MICROBALANCE CONTROL SYSTEMS

The purpose of this chapter is to acquaint the reader with the general background of microbalance technology and describe the development of the automatic controlled null type microbalances. To present this so as to provide an interest to persons dealing with control systems for microbalances, the writer will attempt to describe some of the early achievements with simple balances and then briefly describe some of the more recent techniques for automatic control. As will soon be evident, there are many different methods for automatic control of a microbalance.

This chapter also contains references which will greatly amplify one's knowledge of the applications and varied techniques of precision microgravimetry.

Historical Background

The pioneer work of Emich and Donau[1] contributed immensely to the development of submicrogram measuring techniques. The aim of these pioneer chemists was to develop methods for measuring microgram and submicrogram amounts of material. Although their balances were of limited capacity and performed poorly in high vacuum, they were the forerunners of modern vacuum balances.

---

[1] F. Emich, Lehrbuch der Mikochemie, Munich (1926).

Excellent reviews cover the steady progress in precision microgravimetry from those of Pettersson[2] (1915), through Emich[3] (1921), Gorbach[4] (1936), Ingram[5] (1949), and Kirk[6] (1950).

As the progress of vacuum balance technology continued through the years, various designs of simple balances emerged until they began to group into three different classes. A description of these different types will aid in the understanding of the state of the art viewed in light of recent advances.

The cantilever type[7] of balance determines a weight by measuring the amount of bending of a single fiber, one end being fixed and the other loaded with the substance to be measured. This balance had the virtue of simplicity and adaptability and the drawback of low capacity.

The knife-edge type is a balance with the principle of center point balancing applied. The important advantage to this type of balance is the greater capacity. The first balances of this type employed a true knife edge riding on a flat surface. The technique had the disadvantage of difficulty in reproducing exact measurement since the knife edge had a tendency to slip or change position if the balance beam rotated through a relatively large angle or if the balance beam were not level with respect to the flat plate.

---

[2]H. Pettersson, Proc. Phys. Soc. (London) 32, 209 (1920).

[3]F. Emich, Abderhalden 9, 55 (1919).

[4]G. Gorbach, Mikrochemie 15, 254 (1936).

[5]G. Ingram, Metallurgia 39, 232 (1949).

[6]P. L. Kirk, Quantitative Ultramicroanalysis, New York (1942).

[7]E. Salvioni, Dissertation, University of Messina, (1901).

Later developments[8] vastly improved this type of balance. A quartz fused-on fiber was substituted for knife-edge support of the microbalance. The quartz fiber was used for main support and also for supports for the balance pans.

The spring type balance was originated about 1915 and found widespread use in microanalysis and biochemistry. The spring balance consists of a coil spring suspended vertically in a tube. The load is placed on a pan which is attached to the lower end of the helical spring. The weight is measured by reading the deflection of the spring directly on a graduated scale. The principle of the helical balance, however, imposed a severe limitation on its use, since the ratio of load to sensitivity is limited and relatively small compared to a knife-edge type of balance.

Development of Continuous Null Balance Techniques

As the basic techniques of microgravimetry developed and spread to more fields of study, the need for microbalances with continuous balance or null became more pronounced. For example, in the field of thin film studies it was vital in the deposition of extremely thin layers of metal or other material that weight increase due to this deposition be observed or measured continuously. As a result of these research demands, the automatic microbalance was developed. The development techniques of automatic control, however, took many different routes. Therefore, several different methods evolved for imposing continuous control on the balance beam. This section will describe some of these techniques.

---

[8]B. D. Steele and K. Grant, Proc. Roy. Soc. (London) A82 580 (1909).

Cahn and Schultz[9] reported a microbalance employing automatic control. The deflection of the beam from the null position is sensed by a phototube. The phototube circuit produces an "error" voltage which contains information as to direction and magnitude of deflection. This voltage drives a servo amplifier with necessary compensation and filtering. The rebalancing force is applied to the beam by an elastic-ribbon suspension torque motor.

H. Mayer et al.[10] reported a tungsten torsion microbalance with sensitivity so high that the weight of thin films which consist only of monoatomic layers can be determined. This system utilizes a capacitor bridge, which produces an input signal for the amplifier when the balance departs from the null position. The signal is amplified and demodulated by a phase-sensitive detector. The output signal then passes through a lead network (differentiation) and is applied to the balance through the balance torsion fiber. This signal acts to restore the balance to null position by electrostatic action of three plates, one attached to the balance beam and the other two located in close proximity to the balance plate. These plates, it may be noted, form the capacitors for the capacitor bridge.

H. L. Gruber and C. S. Shipley[11] utilized a continuous null microbalance with still another type of control system. In this system,

---

[9]L. Cahn and H. R. Schultz, Vacuum Microbalance Technique 2 7, (1962).

[10]H. Mayer, et al., Vacuum Microbalance Technique 3 75, (1963).

[11]H. L. Gruber and C. S. Shipley, Vacuum Microbalance Techniques 3 75 (1963).

the beam departing from null is detected by a moving coil technique. This coil movement induces a high frequency signal in the rotating coil. The signal, a function of direction and magnitude of displacement torque, is amplified, rectified in a phase sensitive detector, the resulting d-c amplified and finally returned to the moving coil to restore the beam to null. The balance has a sensitivity of one microgram and a maximum load of one gram. The balance is commercially available and is sold in this country by Brinkman Instrument Company.

C. Norman Cochran[12] assembled a null-type vacuum microbalance with automatic control from commercial components. On the most sensitive ranges, this balance will detect weight changes as small as 0.01 μg with a capacity of one gram. A deflection of the balance beam is detected by a variable permeance transducer. The transducer forms part of an inductive bridge circuit. The output signal from this circuit is the "error" voltage containing the necessary information as to beam position and direction from null. This signal is fed to a servo amplifier. The servo amplifier drives a two phase servo motor connected through a gear train to the balancing potentiometer. This potentiometer together with circuitry which provides range selection has the effect of adjusting the current flow through the compensating solenoid. The compensating solenoid completes the control loop back to the balance beam. It produces the desired force to restore the balance to the null position. The weight read-out is obtained by recording the solenoid current. Czanderna and Honig[13] demonstrated that the change in current through

---

[12]C. N. Cochran, Vacuum Microbalance Techniques 1 23 (1961).

[13]A. W. Czanderna and J. M. Honig, Anal. Chem. 29, 1206 (1957).

the compensating solenoid required to hold the balance at the null position is directly proportional to the weight change of the sample under study.

CHAPTER III

THE DYNAMIC LOAD MICROBALANCE CONTROL SYSTEM

Classification of the System

In order to classify the system upon which the writer based his study, a brief discussion of the general terms and definitions would be in order. As in the other fields of interest, control system technology has developed various words and phrases which are unique to the art.

The term "servomechanism"[1] is defined to mean "a power amplifying device in which the amplifier element driving the output is actuated by the difference between the input to the servo and its output." The word servomechanism, then describes a control system such as is used in the microbalance. The definition above has been broadened in recent years to include a large variety of control systems in which feedback is utilized. Feedback in this sense, means feeding back to the initial stage or stages of the control system a signal proportional[2] to the output.

Control systems may be separated into two distinct types: open-loop and closed-loop. Open-loop control systems cause the output device to perform its task at some predetermined rate, level, et cetera. In

---

[1] H. L. Hazen, Theory of Servomechanisms, J. Franklin Inst. (1934).

[2] Note: The feedback signal may be modified considerably from the actual output signal.

other words, the condition desired is set (quite often manually) at the input of the control system and the output automatically assumes this condition. There is no feedback of the output conditions to the input for comparison in an open-loop system. The accuracy of the output is determined by the calibration of the system. An example of an open-loop control system is a stop light at some street intersection. The lighted period of the lamps and the recycle time is set manually at the input, and the remainder of the control system supplies the necessary power. This system does not "sense" the flow of traffic and regulate accordingly, as a traffic policeman would normally do. Rather, it follows the commands preset at its input.

A closed-loop control system has the same basic components of an open-loop system, but also has other components which distinguish it from an open-loop. The closed-loop system measures the actual output and a signal corresponding to this measured output is compared with the input signal. The control system then acts on command of the resulting "error" signal. The input signal is sometimes called the reference signal or control point setting. In comparison with an open-loop system, it is seen that command of the two systems differs, since in closed-loop operation, the command signal is the signal derived from the comparison of the reference signal and output signal. In open-loop operation the command is preset and does not depend on the characteristics of the output signal. Examples of closed-loop systems included radar antenna control, fire control systems, guidance systems, et cetera.

The dynamic load (implying load change with increasing time) microbalance is a regulating system. When the beam departs from the reference position, or null, the control system acts to reestablish the

beam at the null position; hence a regulator control system. If one restricts the term, servomechanism, to mean only automatic position control, then, referring to Figure 1, the microbalance control system may be called a servomechanism, since unity feedback exists from the output to the input. The error detector (Figure 1) compares a signal which is a measure of the output with the reference signal. This stage or component is the input component of the control system. From the definition of a servomechanism, the microbalance system is a closed-loop control system.

A control system is further classified by looking at the open-loop transfer function. A generalized open-loop transfer function is of the form:

$$G(s) = \frac{K\,(Sa + 1)(Sb + 1)\cdots}{S^n\,(S\tau_1 + 1)(S\tau_2 + 1)\cdots}$$

where K, a, b, T_1, T_2, etc. are constants depending on circuit parameters and N = 1, 2, 3, ·····

Systems are classified by the number of $^1/_s$ terms that appear in the transfer function G(s)[3]. The number N is the exact number of such terms, thus:

N = 0: type 0 system
N = 1: type 1 system
N = 2: type 2 system, etc.

Referring to Appendix A, the LaPlace Transform of an integration operation is the expression $^1/_s$. Thus the type system (0,1,2,etc.) indicates the number of integrations prescribed by the transfer function G(s).

---

[3]Thaler & Brown, Analysis & Design of Feedback Control System, New York, 1960, p. 221.

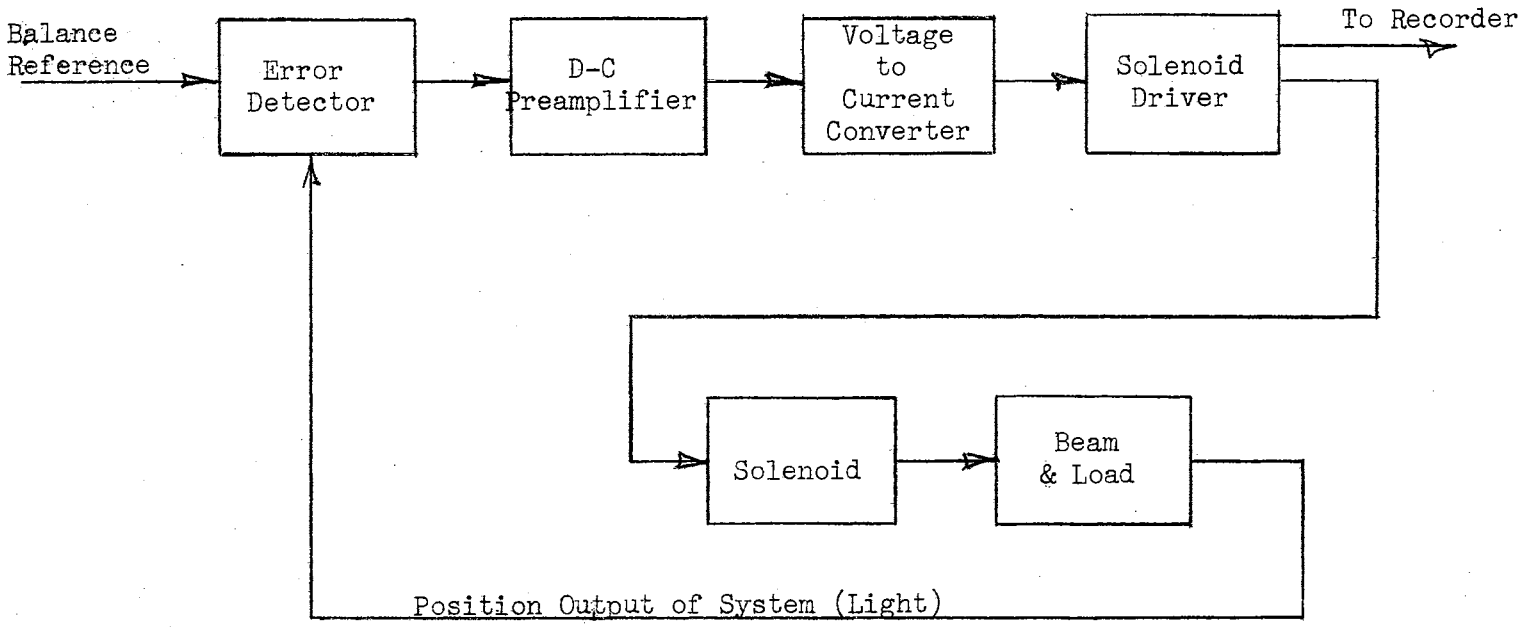

Figure 1. Control Block Diagram

The basic microbalance system is usually a type zero system. The open-loop transfer function equation would then take the form

$$G(s) = \frac{K\,(as + 1)\,(bs + 1)\,\cdots}{(\tau_1 s + 1)\,(\tau_2 s + 1)\,(\tau_3 s + 1)\,\cdots}$$

The exact classification of the system will be verified in later chapters as the actual G(s) for this particular system becomes known.

General Approach to the System Analysis

Any good reference on control system analysis will describe in great detail the currently accepted methods for control analysis. Therefore, the purpose of this section is not to describe the analysis methods. Rather, the purpose is one of bringing to focus upon the microbalance control system a logical procedure or approach to analysis of the performance of this particular control system.

It has been established that the system is a closed-loop system with unity feedback. Therefore several methods of analysis are possible, including root-locus methods, Nyquist Criteria, frequency response methods. Therefore, the approach one should take is to set forth exactly what characteristics of the system must be determined, then develop a logical procedure to expose these characteristics.

The first characteristic of the microbalance which required examination was the stability of the control system. After stability has been established, then one would like to know exactly what margin of stability exists. In other words, how much may the parameters of the system, such as gain, be changed and still maintain a system with stable performance? The third question to be answered would be: what is the

steady-state error of the system? This question may be answered only after stability and other characteristics are known.

The performance of the microbalance control system could very well be determined solely by mathematical manipulation of system equations. However, due to the complexity of the components involved, the basic system equation, the open-loop transfer function, is not known nor is it readily derived. Some components of the system contain circuitry which would greatly affect the system transfer function. These component transfer functions could be determined only by experimental techniques. Therefore, some other approach must be taken to analyze the microbalance system.

It was decided, in view of the lack of system equations, to examine the control system from the frequency response standpoint. The frequency response of the forward loop of the control system may be determined experimentally in much the same way as a single component would be tested. The frequency response characteristics of the forward-loop, when displayed as a Bode diagram,[4] will yield the necessary information as to system stability. The Bode diagram will also give the necessary information as to stability margins. Finally, the results of the frequency response tests will provide the information necessary to determine system steady-state error.

---

[4] Ibid., p. 154.

CHAPTER IV

DESCRIPTION OF THE MICROBALANCE

General

The system which this writer chose to investigate is utilized in high temperature metal studies. In particular, the microbalance is used to measure the change of weight of a vaporizing sample. The sample is contained in an inverted Knudsen cell, as shown in Figure 2. As the sample is heated, the vaporized metal flows out of the Knudsen cell through the orifice. The change of weight results as vapor flows from the container into the furnace chamber. The change of weight range depends on running time, temperature, and type of sample. The flow through the orifice leads to another important measurement--the measurement of the force of the molecules of vapor flowing from the orifice. This reaction force is also in the microgram region. This reaction force is observed when heating is terminated and vapor flow ceases.

The microbalance upon which this thesis is based is a balance which was developed in a research laboratory and specially designed to fit the needs of the research program. It is incorporated in a vacuum system which may be evacuated to pressures of 1×10^{-6} mm of mercury. A vacuum pumping system which includes a mechanical pump and a diffusion pump was utilized. The entire system with the exception of the

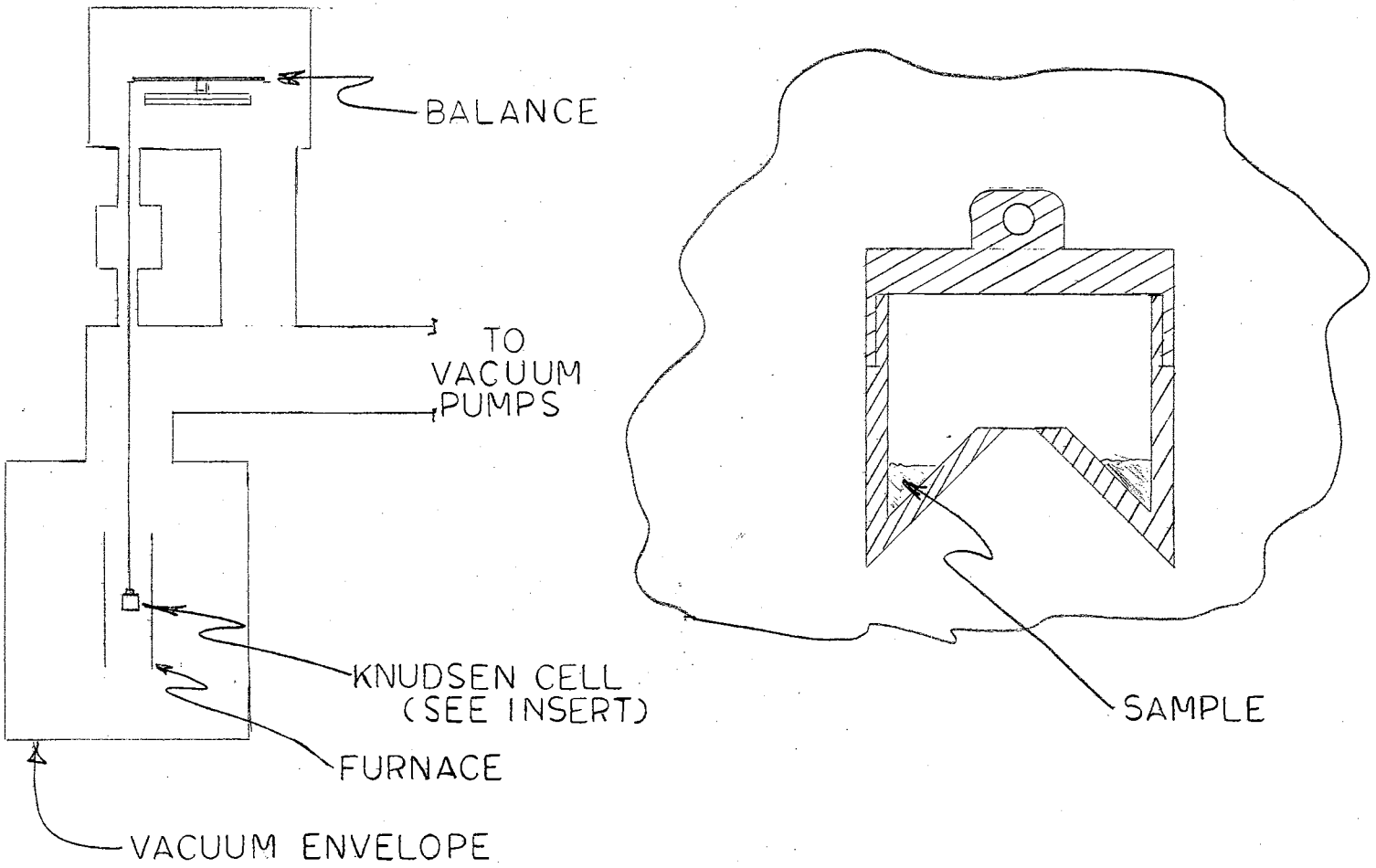

Figure 2. The Inverted Knudsen Cell

mechanical pump and the electronic control system is mounted on a large concrete block by cantilever support. This technique allowed a means of minimizing vibrations in the balance structure.

The complete microbalance system then, involves a high temperature furnace, a specially designed vacuum system, a beam balance with an inverted Knudsen cell sample holder, and a control system. The control system provides, as an integral part, means of visual read-out of change of sample weight from some prescribed null or balance point. The complete system is shown in Figure 3. Since the purpose of this study is the analysis of the control system of the microbalance, components of the total system which do not have a direct bearing on system control will not be discussed in any detail. However, effects on the control parameters by non-control components such as the furnace and the vacuum system will be discussed at the appropriate time in subsequent chapters.

The Beam Balance

A detailed description of the control system would naturally start at the beam balance. The purpose of the control is to hold the beam at continuous null. In other words, as weight is lost from the sample, a counterweight (electrical in this case) must be added to maintain the beam of the balance in a stationary position.

The beam balance may be described as follows: the beam, fabricated from stainless steel, rides on a diamond-sapphire pivot; the Knudsen cell is suspended by a fine metal wire from diamond point contact points; the precision adjustable counterweight is provided by a hanging chain tare adjustment. A detailed drawing of the beam balance is shown in Figure 4. Two other features which are directly related to system

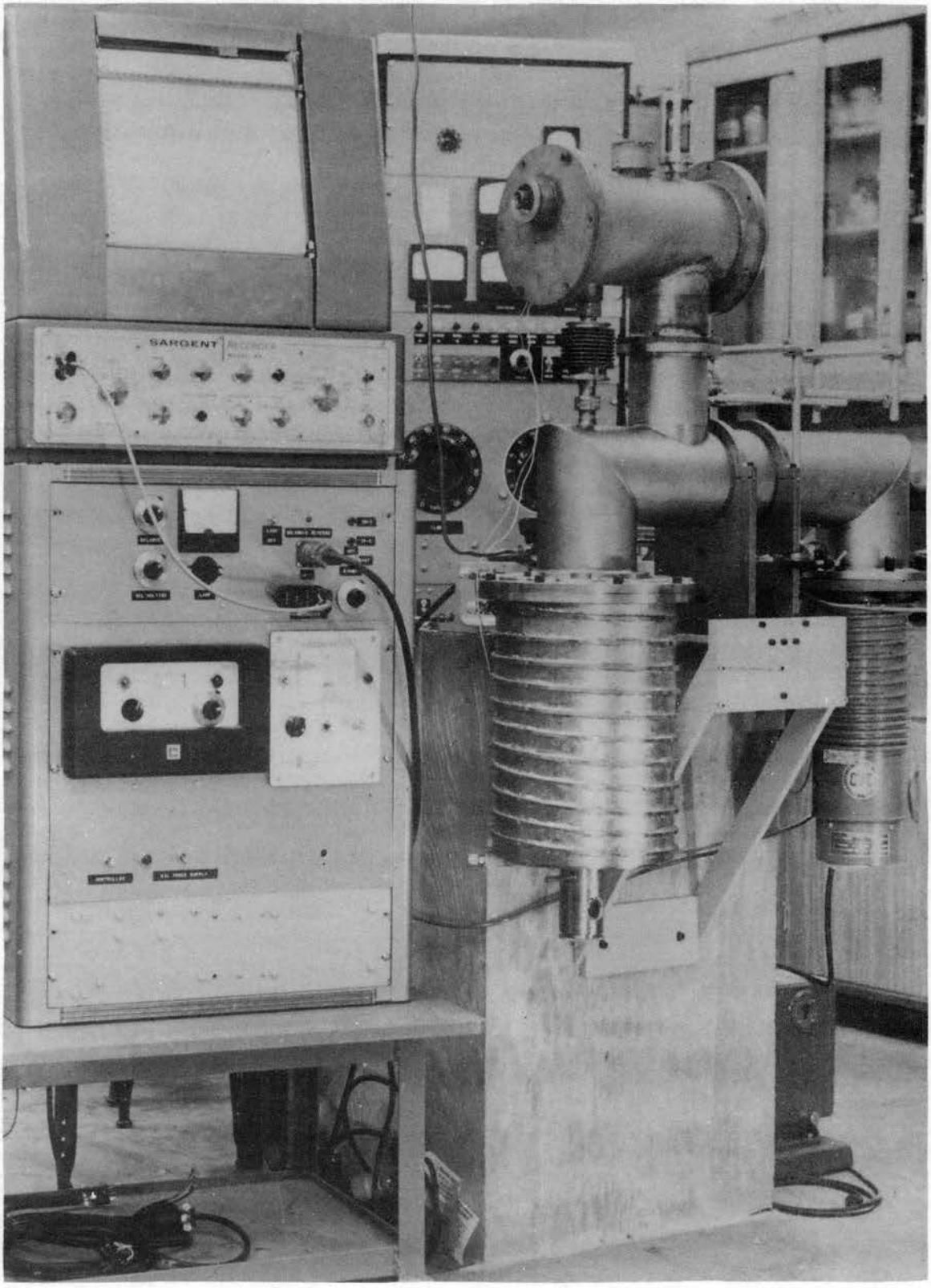

Figure 3. The Automatic Vacuum Microbalance

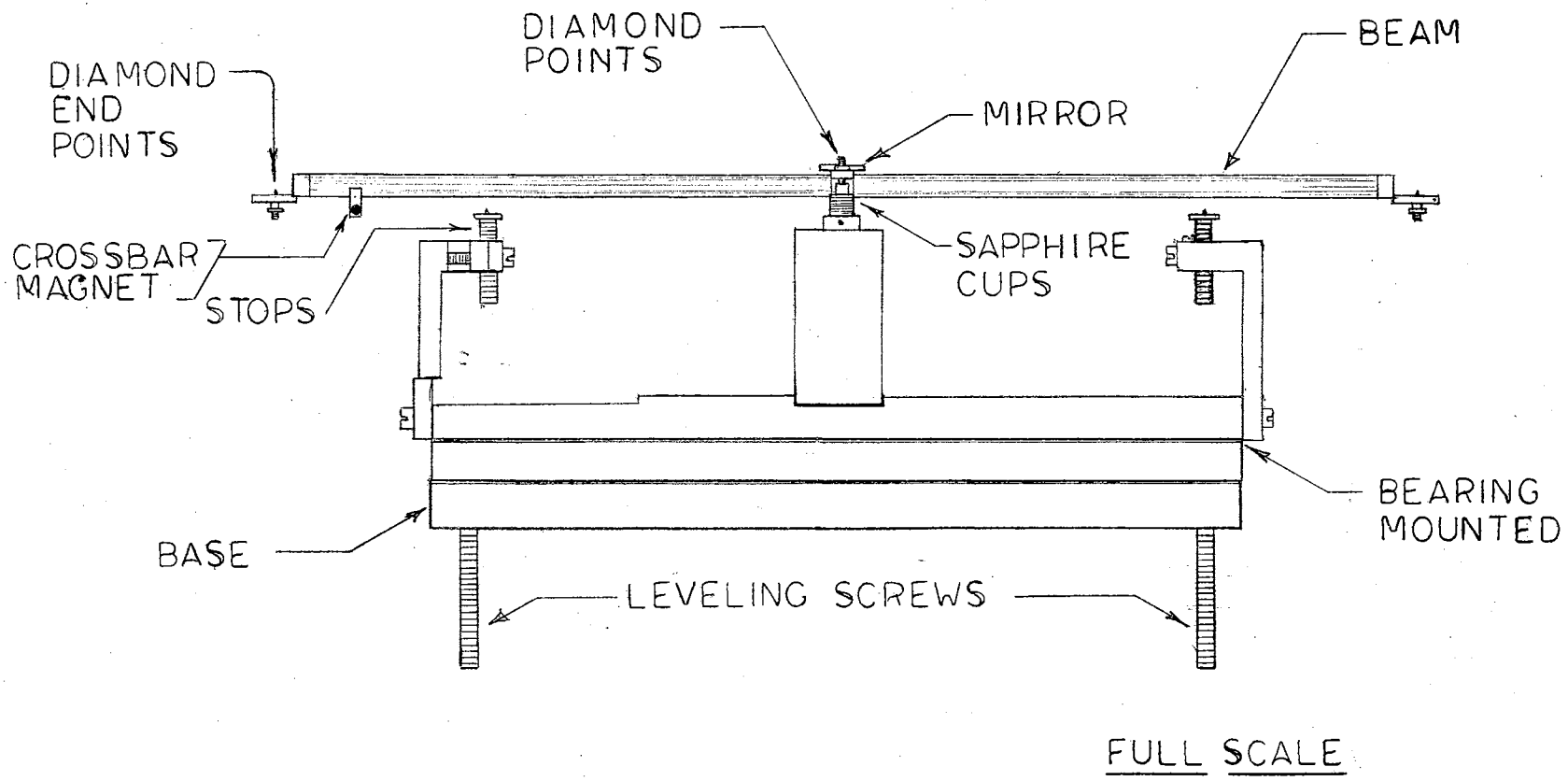

Figure 4. Balance Beam and Mount

control are the beam mirror and the crossbar magnet. The mirror reflects the spot of light utilized in the error detector circuitry and the crossbar magnet provides coupling between the beam and the solenoid. The magnet also introduces some damping which will be discussed in more detail later in this study.

Error Detector

It is the purpose of the error detector to detect a change in the position of the balance beam and produce an output signal describing this change. Output of this circuit must contain two bits of information, namely, the direction of change and the instantaneous distance of the beam from the null point.

The complete error detector is shown in Figure 5. The primary light source is a projection lamp. The light is transmitted through fiber optics to a position directly above the mirror which is mounted on the balance beam. The light is then reflected up through a lens system to the photopot. The spot of light which strikes the photopot performs the same function as a slider in a conventional potentiometer or variable resistor. The photopot forms two legs of a bridge circuit. A simplified drawing of this bridge network is shown in Figure 6. The output of the bridge circuit is a voltage which is proportional to the distance of the balance beam from null. The polarity of the output voltage is an indication of the direction in which the beam is displaced from null.

The photopot was selected as the conversion component after testing and actual service of other devices. A photo cell arrangement as shown in Figure 7 was tested. Although satisfactory output signals were obtained, this arrangement had the disadvantage of requiring a sharply

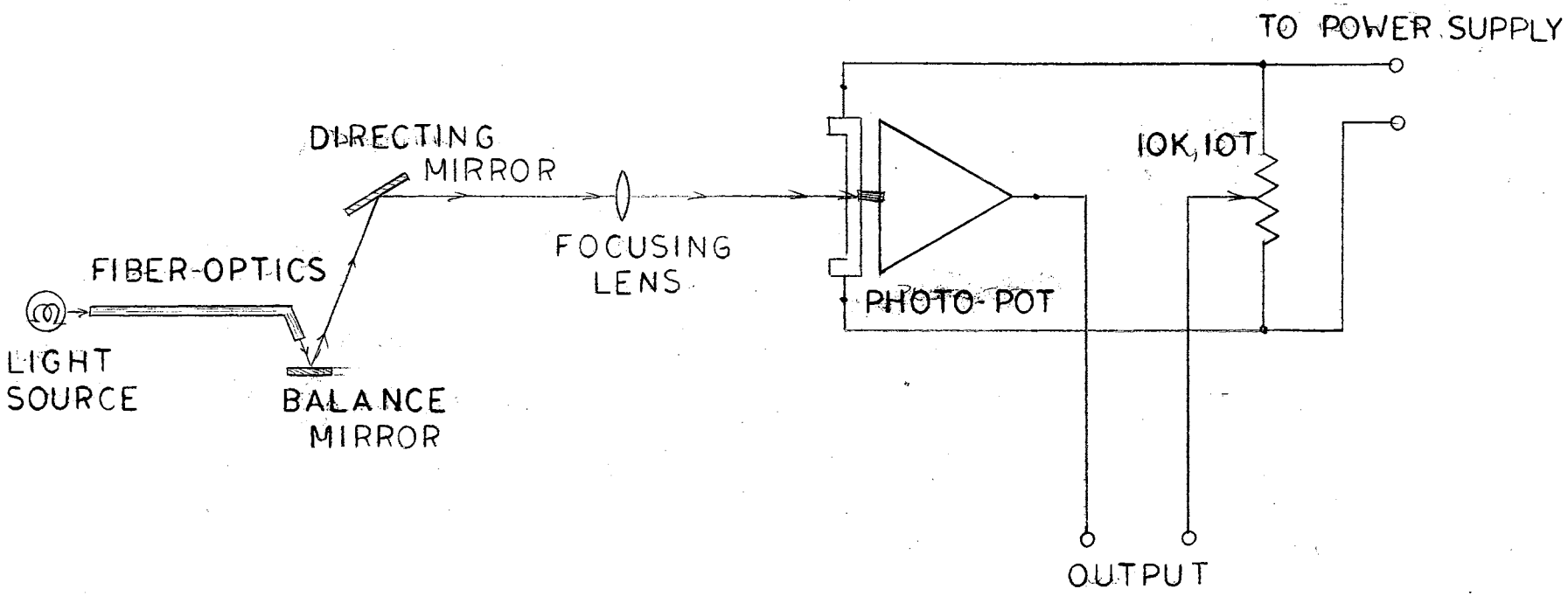

Figure 5a. Error Detecting System

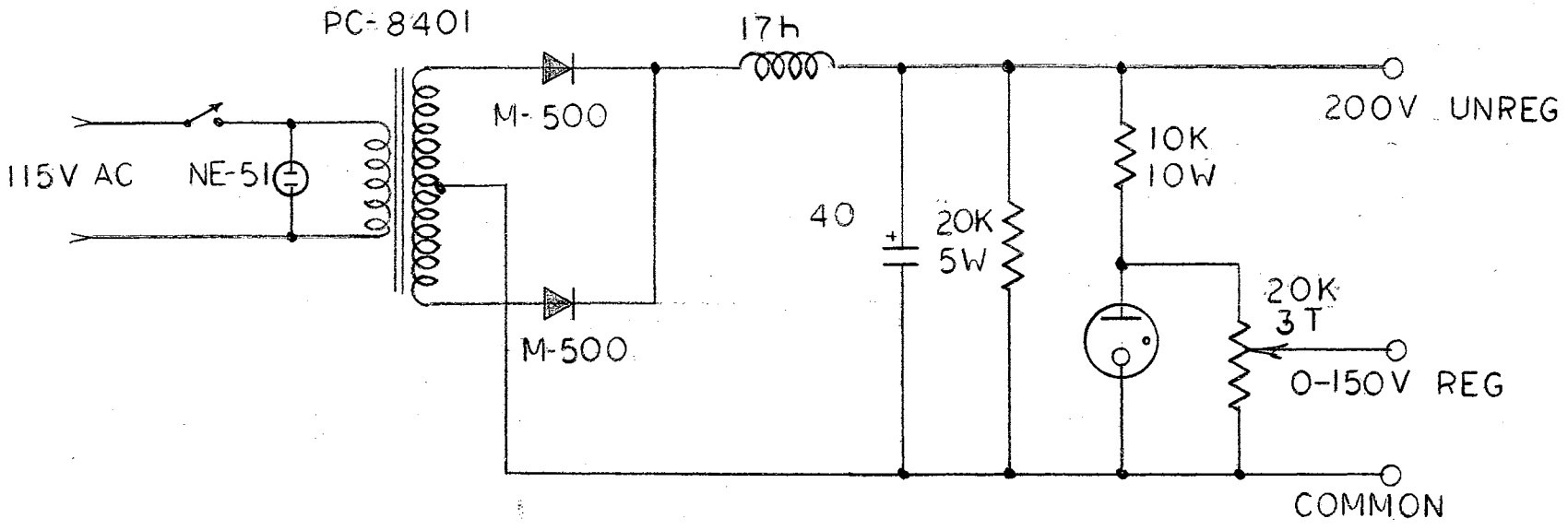

Figure 5b. Error Detector Power Supply

*GIANNINI CONTROLS CORPORATION

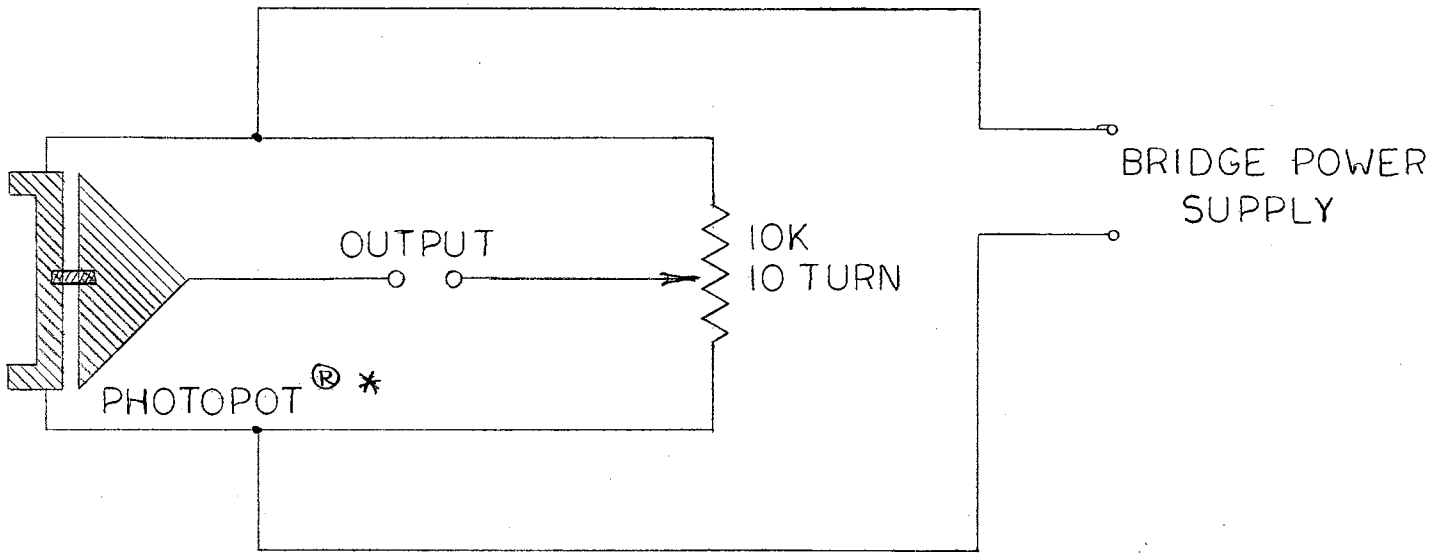

Figure 6. Error Detector Bridge Circuit

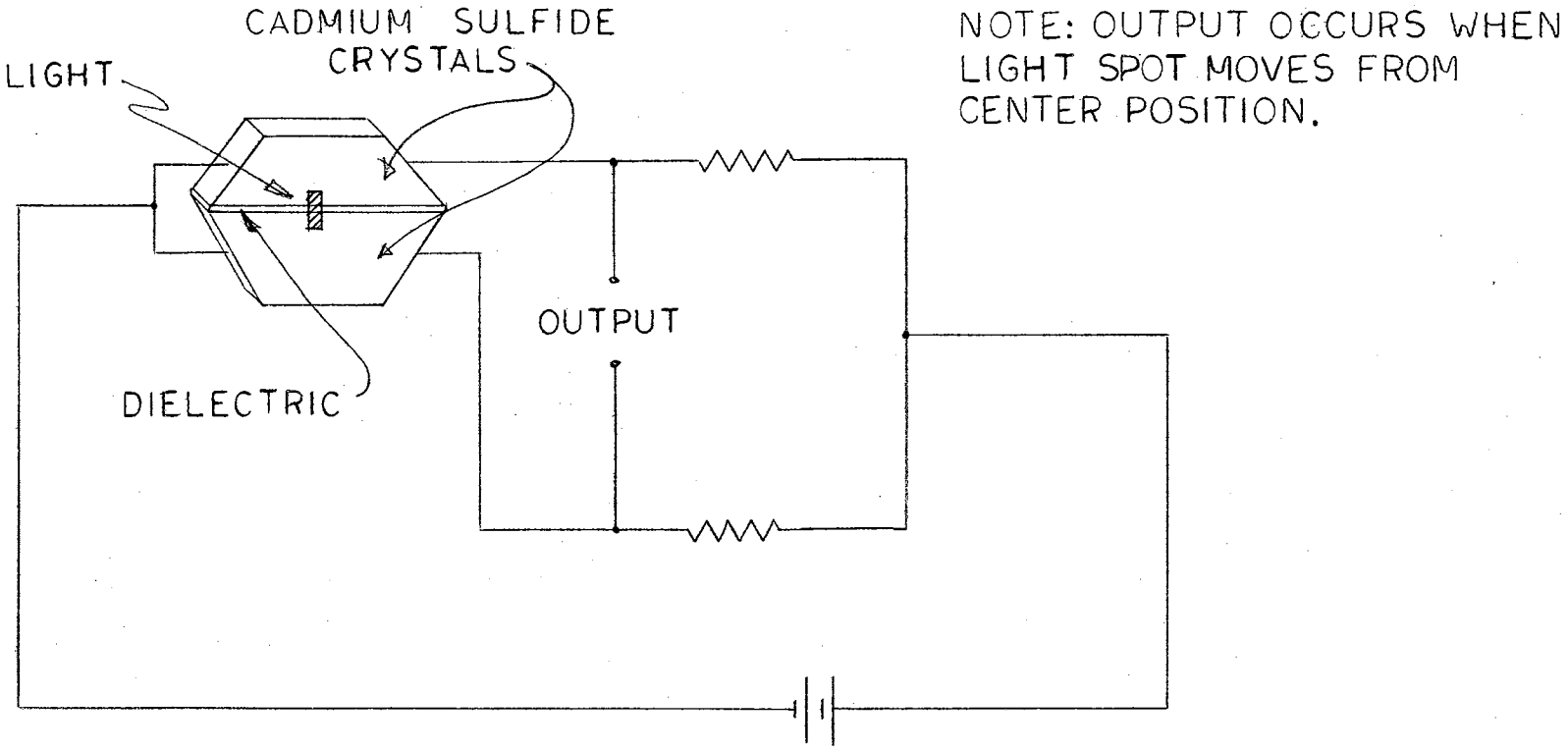

Figure 7. Photocell Detector

focused slit of light for satisfactory performance. The photopot on the other hand, performed extremely well with a less critical source of light.

The error detector offers two important control parameter adjustments. The amplitude of output voltage for a given beam displacement is fully adjustable by simply changing the voltage across the bridge circuit. Also, the rate of change of output voltage for a change in beam deflection may be adjusted by varying the length of the light arm. The importance of these adjustments will become apparent in the following chapter.

The D-C Preamplifier

In order to increase the sensitivity of the microbalance, the output of the error detector must be amplified. The amplifier must be an extremely stable d-c amplifier with excellent zero drift characteristics. In the construction of the microbalance utilized in this study, the decision was made to purchase a commercially available d-c amplifier rather than fabricate one in the laboratory. The amplifier chosen was a Leeds and Northrup d-c null detector. This particular amplifier has several advantages over standard operational amplifiers. It has visual read-out of output voltage. Also, it has adjustable gain and an output limiting circuit. The specifications of the null detector are shown in Table I.

Referring to Figure 8, the d-c null detector operates the same as a standard d-c amplifier with a few exceptions. The input circuit employs a three stage R-C filter circuit to minimize the a-c interference developed across the input leads. D-c to a-c conversion is accomplished

TABLE I

Specifications of the D-C Preamplifier

MAXIMUM SENSITIVITY

Sensitivity decreases linearly as source resistance increases.
at source resistance of 1,000 ohms:
0.67 microvolt per millimeter
1.0 microvolt per scale division.
at source resistance of 100,000 ohms:
2.3 microvolts per millimeter
3.5 microvolts per scale division.

ZERO DRIFT

Conditions: 30-minute warmup before operation, temperature of 68 ± 10F, max. gain.
During first hour of operation--less than 1.5 divisions
After three hours operation--less than 0.5 division

NOISE LEVEL

Less than 0.2 microvolt, peak to peak

SPEED OF RESPONSE

Less than 2 seconds for source resistances up to 1,000 ohms, increasing to 4 seconds at 100,000 ohms.

INPUT RESISTANCE

25,000 ohms

OUTPUT IMPEDANCE

1,000 ohms

OUTPUT

-.5 volt to + .5 volt

LINE VOLTAGE REQUIRED

120 volts, 50/60 cycles

POWER CONSUMPTION

18 watts

WEIGHT

approximately 16 pounds

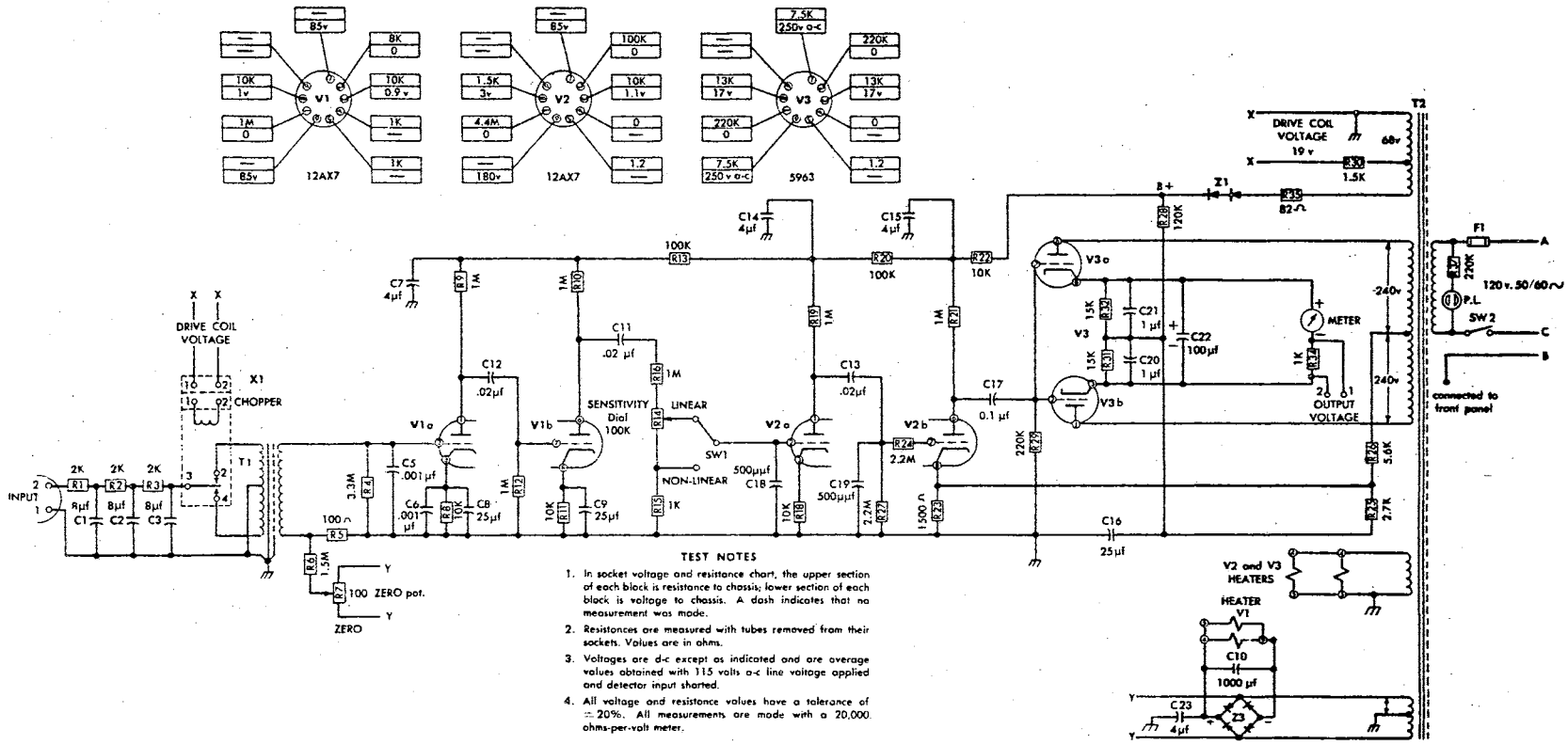

Figure 8. The D-C Preamplifier Circuit

by means of a contact vibrator. The converter, in conjunction with the input transformer, T-1, produces an a-c signal which is proportional in magnitude to the magnitude of the input d-c signal. The phase of the resulting a-c signal is related to the polarity of the d-c input signal. A reversal of the input d-c signal results in a 180 degree phase shift of the a-c signal.

After conversion, the resulting a-c voltage is amplified by a total of four consecutive voltage stages employing conventional R-C coupling. These stages are standard in design with a few exceptions. Because low level a-c signal appears at the input, precautions must be taken to avoid noise and transient interference. Therefore, the first stage employs d-c current for its heaters, and capacitors are utilized to short transient voltage for frequencies higher than 60 cycles per second. These capacitors are in the first stage.

The third and fourth stages have degenerative feedback. This is effected by leaving the cathode resistors unbypassed. The fourth stage also has feedback from the a-c to d-c conversion stage.

The last stage of the null detector is the a-c to d-c conversion. This is done electronically. The stage employing V-3 performs the conversion. This stage is sensitive to both the magnitude and phase of the input a-c signal. The resulting d-c output will be positive or negative depending on the phase relationship and the magnitude of the d-c is proportional to the magnitude of the a-c.

Voltage to Current Converter

The amplified error voltage must be transformed to a current signal which is proportional to the error voltage. The transformation is necessary for the following reasons: the d-c preamplifier is not capable of producing output currents large enough to drive the solenoid driver; the solenoid driver requires a zero to five ma current to utilize its full range.

The voltage to current conversion is accomplished by utilization of a process control unit manufactured by Leeds and Northrup (Figure 9). In addition to conversion, this unit provides adjustments of some control parameters.

In general, this unit was designed for process control and therefore it has some features which are not used in the control of the microbalance. The input circuitry contains, as an integral part, a bridge power supply and part of a bridge circuit. This is normally used in conjunction with a control slide wire in process control.[1] This particular feature is not used in the microbalance control system. Also, the control unit provides connections for a safety switch and electro-pneumatic converter coil. These features were obviously not used in the microbalance system.

The modification of the control unit described above was very simple owing to the fact that all of the connections for power, safety switches, input, and output were conveniently located on a back panel. Therefore, utilization of jumper bus plates rendered the control unit

---

[1]Series 60 control using three-action C.A.T. control, unit Leeds and Northrup 077993.

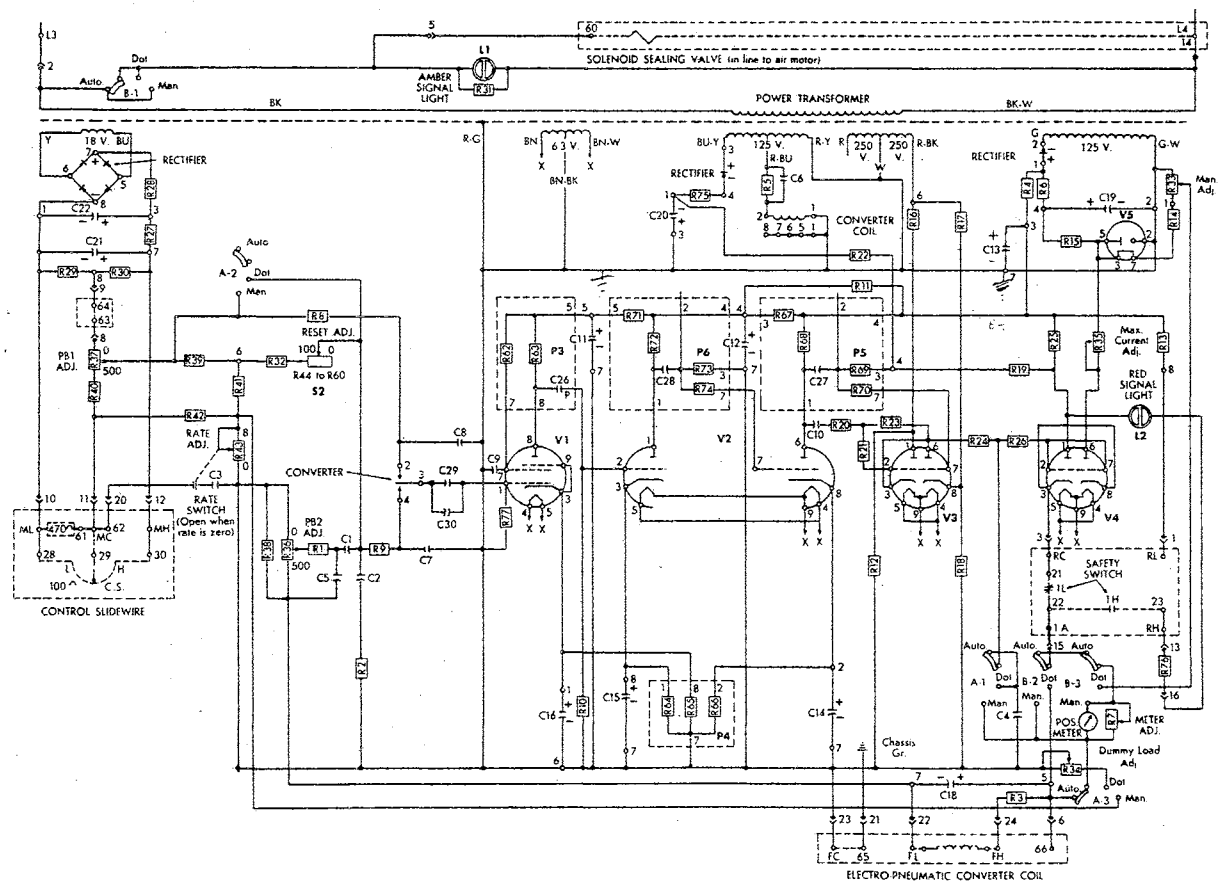

***RESISTORS**

			Part No.
R1	6.8K		11-1-0-54
R2	2.7K		11-1-0-49
R3	1K		11-1-0-44
R4	1K		11-1-0-44
R5	2.7K	2W	11-3-0-49
R6	470Ω		11-1-0-40
R7	1K		013150
R8	2.2M		11-1-0-84
R9	.47M		11-1-0-74
R10	2.2M		11-1-0-84
R11	1M		11-1-0-68
R12	.68K	1W	11-2-0-66
R13	22K	1W	11-2-0-60
R14	4.7K		11-1-0-52
R15	2.2K	2W	11-3-0-48
R16	22K		11-1-0-60
R17	.68K	1W	11-2-0-66
R18	33K		11-1-0-62
R19	820K		11-1-0-79
R20	.33M		11-1-0-74
R21	1M		11-1-0-80
R22	.27M		11-1-0-73
R23	.27M		11-1-0-73
R24	33K		11-1-0-62
R25	33K		11-1-0-62
R26	.1M		11-1-0-68
R27	22Ω	2W	11-3-0-24
R28	22Ω	2W	11-3-0-24
R29	510Ω		11-11-0-6
R30	510Ω		
R31	1M		11-1-0-80
R32	15K		11-1-0-58
R33	10K		13-2-0-10
R34	10K		013145
R35	10K		
R36	10K		013140
R37	2K		
R38	2.7K		11-1-0-49
R39	820Ω		11-1-0-43
R40	270Ω		11-1-0-37
R41	180Ω		11-1-0-35
R42	10K		11-1-0-56
R43	2M		013141
R44	68M		11-1-0-102
R45	27M		11-1-0-97
R46	22M		11-1-0-96
R47	10M		11-1-0-92
R48	6.8M		11-1-0-90
R49	2.7M		11-1-0-85
R50	2.2M		11-1-0-84
R51	1M		11-1-0-80
R52	.68M		11-1-0-78
R53	.27M		11-1-0-73
R54	.22M		11-1-0-72
R55	1M		11-1-0-68
R56	68K		11-1-0-66
R57	27K		11-1-0-61
R58	22K		11-1-0-60
R59	10K		11-1-0-56
R60	82M		11-1-0-103
R76	2.7K		11-1-0-49
R76	.33M		11-1-0-74
R77	82M		11-1-0-103

*All resistors are ½ watt with ± 10% tolerance except as specified.

†For chassis 354162 only. Converter for chassis 354181 is Part No. 354169.

▼Supplied as parts of S2.

COLOR CODE

BK – Black	OR – Orange
W – White	Y – Yellow
G – Green	GY – Gray
R – Red	PU – Purple
BU – Blue	PK – Pink
BN – Brown	LBU – Light Blue

CAPACITORS

			Part No.
C1	10µf	10vDC	023118
C2	24µf	5vDC	023119
C3	24µf	5vDC	
C4	5µf	100vDC	023120
C5	.5µf	200vDC	23-3-0-23
C6	.5µf	200vDC	23-3-0-23
C7	.05µf	400vDC	23-3-0-9
C8	.05µf	400vDC	23-3-0-9
C9	.1µf	400vDC	23-3-0-8
C10	.022µf	400vDC	23-3-0-20
C11	4µf	200vDC	
C12	4µf	200vDC	
C13	4µf	200vDC	23-2-0-17
C14	25µf	2vDC	
C15	25µf	2vDC	
C16	25µf	2vDC	
C17	50µf	3.5vDC	
C18	12µf	210vDC	23-2-0-18
C19	4µf	300vDC	
C20	4µf	300vDC	
C21	1000µf	12vDC	023121
C22	500µf	20vDC	
C29	.001µf		023125
C30	.001µf		

PRINTED CIRCUITS

			Part No.
P3	R62	2.2M	144012
	R63	.47M	
	C26	.002µf	
P4	R64	15K	144011
	R65	6.8K	
	R66	15K	
P5	R67	1M	144013
	R68	.47M	
	R69	1M	
	R70	1M	
	C27	.002µf	
P6	R71	1M	144013
	R72	.47M	
	R73	1M	
	R74	1M	
	C28	.002µf	

MISCELLANEOUS

		Part No.
S1	Auto.-Man. Switch	031135
S2	Reset Switch	032182
L1	Amber Light	26-1-0-7
L2	Red Light	26-1-0-8
M1	Positive Ind. Meter	020006
V1	5879 Tube	22-1-0-15
V2	12AX7 Tube	22-1-0-6
V3	12AX7 Tube	22-1-0-6
V4	5963 Tube	22-1-0-7
V5	0A3 Tube	22-4-0-2
X1	Converter†	354156
Y1	Rectifier	057017
T1	Transformer	019184
N1	Low Level Cable	037333
N2	High Level Cable	
N3	Converter Cable & Cap	037253

NOTE: Terminal and switch designations in external equipment (shown dotted) apply to Speedomax M. For designations on Speedomax G or Micromax, refer to installation wiring diagram.

Figure 9. Diagram of Voltage to Current Converter

capable of the desired voltage to current conversion.

The converter may be described best by dividing it into three distinct components--the input circuitry, the converter and amplification stages, and the demodulation circuitry.

The input circuitry (Figure 9) contains most of the elements which adjust control system parameters. These adjustments are mounted on the front panel of the unit and include: proportional control, automatic reset, and rate time adjust.[2] The proportional control is a control action in which the change of process input is proportional to the indicator "band" width.

The automatic reset provides floating correction of process input at a speed proportional to the deviation of the indicator from the control point setting.

Rate time applies a correction to the process input which is proportional to the rate of change of the indicator from control point setting.

The converter and amplification section of this unit follows conventional patterns in that conversion is performed by a standard mechanical vibrator and the resulting a-c is amplified by capacitive coupled amplifier stages. The converter is capacitively coupled to the first amplification stage, V-1. The a-c signal is then further amplified by the two following stages. V-2, a high gain dual triode make up the final two stages of amplification (Figure 9).

The demodulation of the amplified a-c signal is performed in the stage made up of the two sections of V-3. The resulting d-c level

---

[2]Series 60 C.A.T. control unit, Leeds and Northrup 077993.

adjusts the current magnitude flowing through V-4, the final stage. This stage (V-4) provides the output current; zero to five ma. The maximum output current is set by adjustment of the variable resistor connected between one of the plates of V-4 and the regulated (V-5) power supply.

The input circuitry and the feedback circuits in this unit make it extremely difficult to predict the exact transfer function. The performance of the total system will depend on the control settings of this unit. However, as will become evident in the following chapters, the effects of the compensatory devices in this unit will be experimentally determined and adjustments made accordingly.

Solenoid Driver

The converter produces a current as described in the preceding section. This control current must be amplified before it arrives at the solenoid. The solenoid was designed to operate between its approximate limits of 5 to 100 ma. This current range is necessary to establish a magnetic field strong enough to control the position of the balance beam. Since the converter can only provide zero to five ma with a suitable load, it is obvious a current amplifier is required.

The amplifier chosen to perform this task is depicted in Figure 10. This amplifier, or solenoid driver, loaded by the solenoid coils, provides a linear output of 0 to 100 ma for a control input of zero to five ma. As may be deduced from the figure, the solenoid driver operates on the magnetic amplifier principle.

To understand the circuit shown, a brief discussion of the theory of operation of a magnetic amplifier would be helpful.

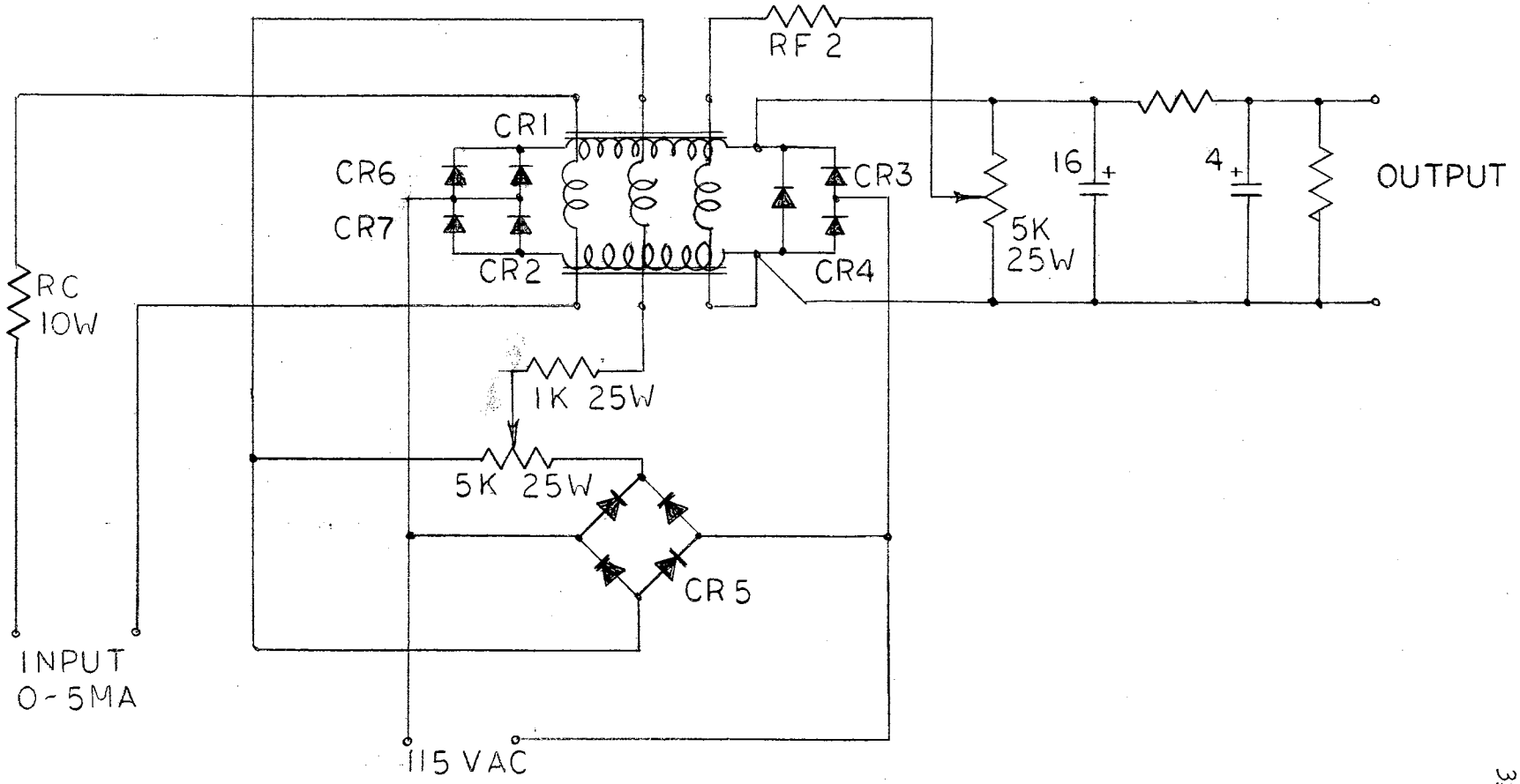

Figure 10. Diagram of Solenoid Driver

The basic magnetic amplifier circuit (Figure 11) involves a core of magnetic material, bias winding (d-c), control winding (d-c), feedback winding (d-c), two a-c windings, and a rectifier circuit. The magnetic amplifier is essentially a variable impedance control of power to the load. By controlling the saturation of the core, the voltage across the load may also be controlled. The current through the bias winding is of such a magnitude as to saturate the core, thus offering a high impedance to the a-c voltage source. Therefore, the voltage drop across the load is at a minimum. The control winding (Figure 11) is wound in an opposite direction from the bias winding, so that an increase in control current will bring the core out of saturation. In a non-saturated condition, the core offers a low impedance to the a-c source and therefore the voltage across the load is maximum.

The magnetic amplifier has good gain characteristics because the power is delivered from the a-c source and the input (control winding current) need only vary a small amount to vary the output voltage over its entire range. The feedback winding (negative or regenerative) has the effect of lowering the gain of the amplifier but offers amplifier stability and a more linear operation over its output range.

The magnetic amplifier employed in the microbalance system (Figure 10) has provisions for adjusting the bias current level and the feedback current level. This provides a means of adjusting the linearity, stability, and gain to an optimum setting.

The Solenoid

The solenoid acts as the final link between the control system and balance beam. The electrical "counterweight" prescribed by the error

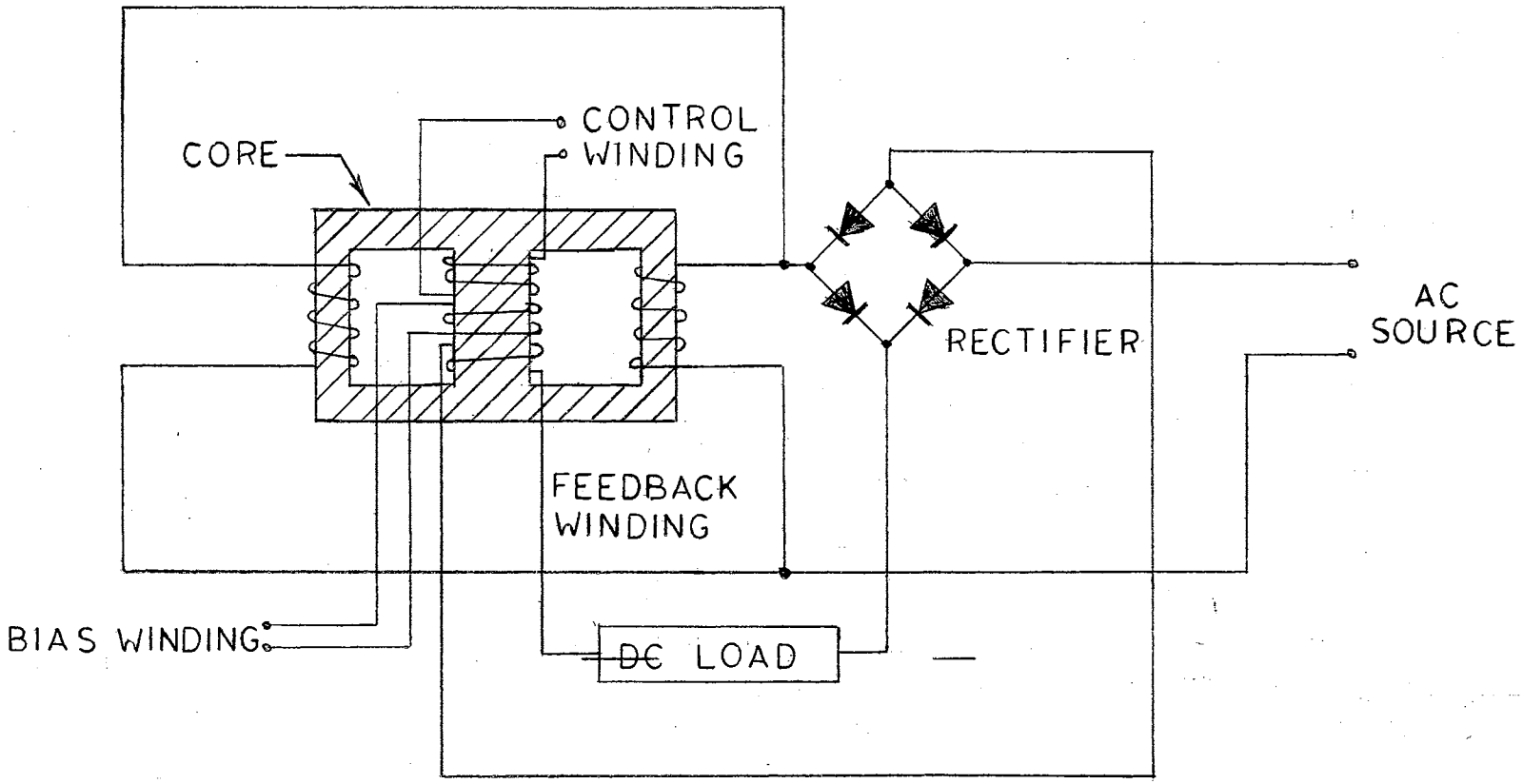

Figure 11. Diagram of Basic Magnetic Amplifier Circuit

is magnetically coupled to the balance beam. This is accomplished as follows: A small crossbar magnet is attached to one end of the balance beam (the load end). This magnet is located in an optimum position between four coils which comprise the solenoid. The magnetic flux of the solenoid cuts the crossbar magnet and a net force or, in this particular case, a torque is applied to the balance beam. A photograph of the balance beam showing the location of the four coils with respect to the beam and crossbar magnet is depicted in Figure 12. Each coil is made up of 2000 turns of number thirty copper wire wound on a solid copper form. The copper forms were used to provide good I^2R heat dissipation since the coils are mounted in an evacuated cylinder which offers very little convection cooling. The forms are triangular in cross-section which allows closer positioning of the coils to both the beam and the crossbar magnet.

The wiring diagram of the coils is shown in Figure 13. Notice the polarity of the individual windings. To produce a net downward (or upward) force and hence a torque on the beam, the pair of coils on the north pole of the magnet must be opposite in polarity to the pair of coils on the south pole end of the magnet. Connected as in Figure 13, all four coils produce forces in the same direction, hence delivering maximum torque in the balance beam. Of course, the torque will be a function of the current through the coils.

The electrical leads to the solenoid are passed through the vacuum cylinder wall by a vacuum-tight electrical feed-through connector.

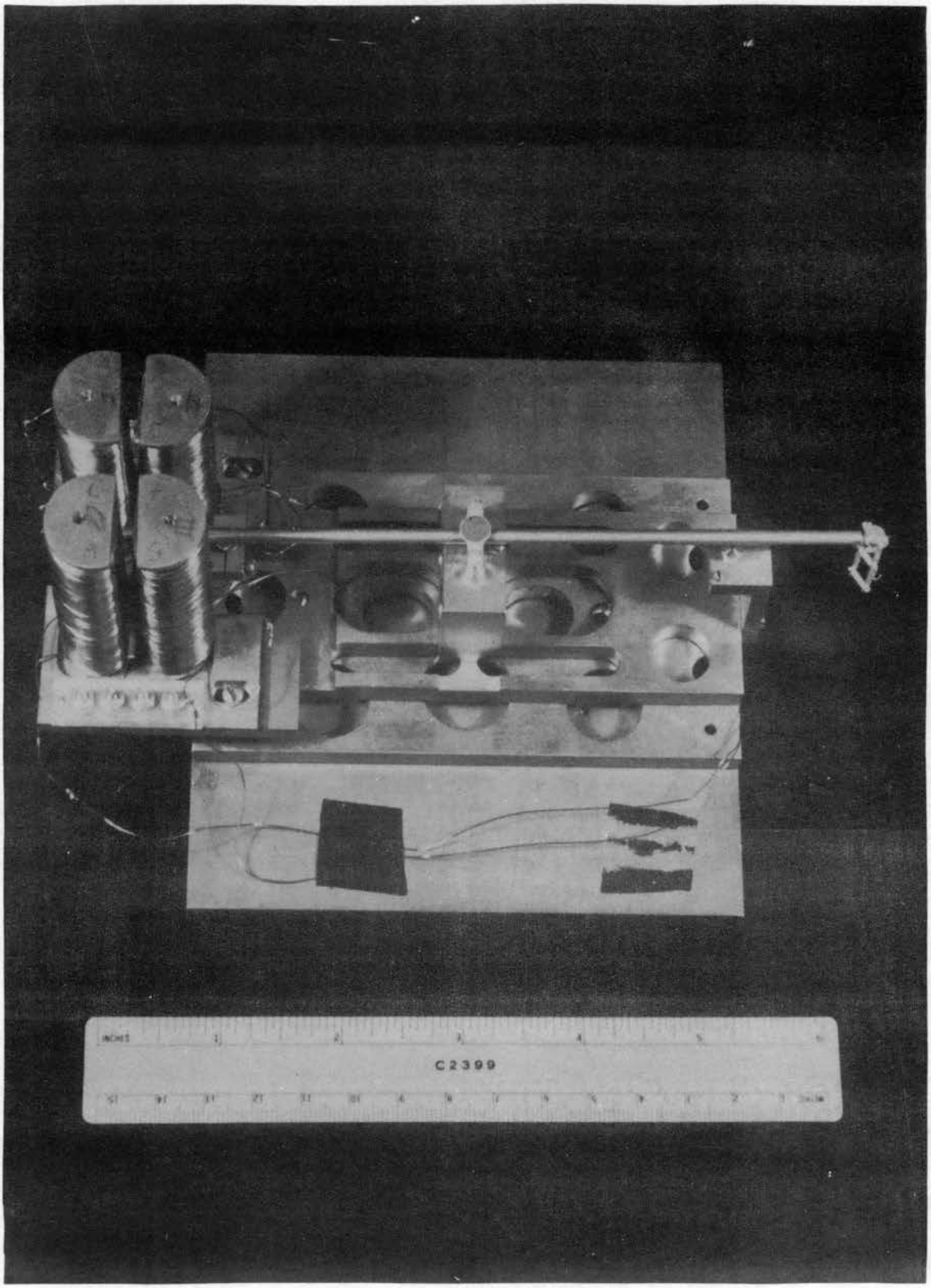

Figure 12. The Beam Balance

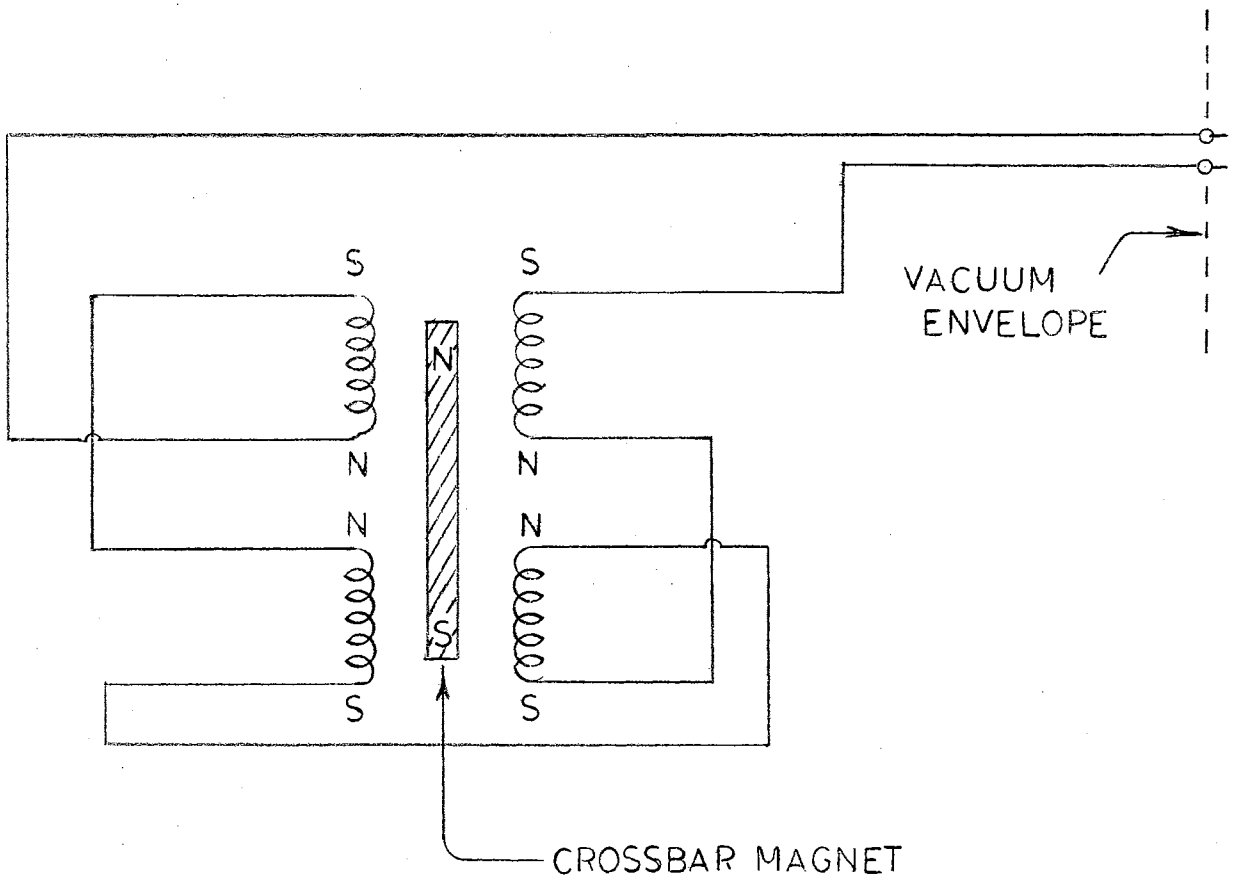

Figure 13. Wiring Diagram of the Solenoid

CHAPTER V

ANALYSIS OF THE SYSTEM

The information obtained from the characteristics of the open-loop response of the control system provides a means of determining system stability. Also, this information can be used to synthesize the system transfer function. At the same time, nonlinearities, if any, will become evident. After the stability and other system characteristics have been determined, then improvement of the transient response, static error, et cetera, of the system may be performed. The use of compensation devices may be introduced to adjust and improve the system's performance.

Procedure for Obtaining Bode Diagram

The first step, then, is to obtain a Bode plot of the frequency response of the system. The plot of gain magnitude and the phase angle versus frequency will yield important information as to the gain margin and phase margin of the system. Also, from the plot of the gain magnitude, a good approximation of the system transfer function may be obtained. The Bode diagram may be obtained by considering the following. The output of the error detector is an indication of the balance beam position with respect to the null reference position. If the balance beam were driven sinusoidally at very low frequencies (that is, frequencies less than the natural frequency of the balance), then the output of the error detector will be a sine wave similar to the driving

voltage, but with this important difference; the output sine wave will differ in phase and magnitude due to the characteristics of the system. A plot or recording of the input driving signal and the error detector versus time as the driving frequency is varied will yield the information necessary to construct a Bode diagram. For each chosen frequency, the gain magnitude and phase difference may be extracted and plotted versus log ω.

A low frequency oscillator, with variable frequency output (HP202A) was used to drive the control system. The driving signal and the resulting system output was recorded on a two-channel Sanborn recorder. A diagram of the testing procedure is shown in Figure 14.

Results of the Test

The test on the system was performed after careful alignment of the optics system and adjustment of circuit gain and the bridge voltage. The output of the low frequency oscillator was set at a constant voltage output of 6.7×10^{-3} volts for the entire frequency range. This offered an advantage in the calculations of the gain magnitude for the Bode diagram.

The input signal and output signal was recorded for various frequencies on the dual channel recorder. The recorder displayed the signals in exact real time correspondence. Therefore, at some arbitrary time, t_o, the phase difference may be read directly from the chart paper. The gain magnitude (peak to peak) may also be read directly from the chart. An example of the recording chart paper showing the phase and gain difference between input and output is given in Figure 15.

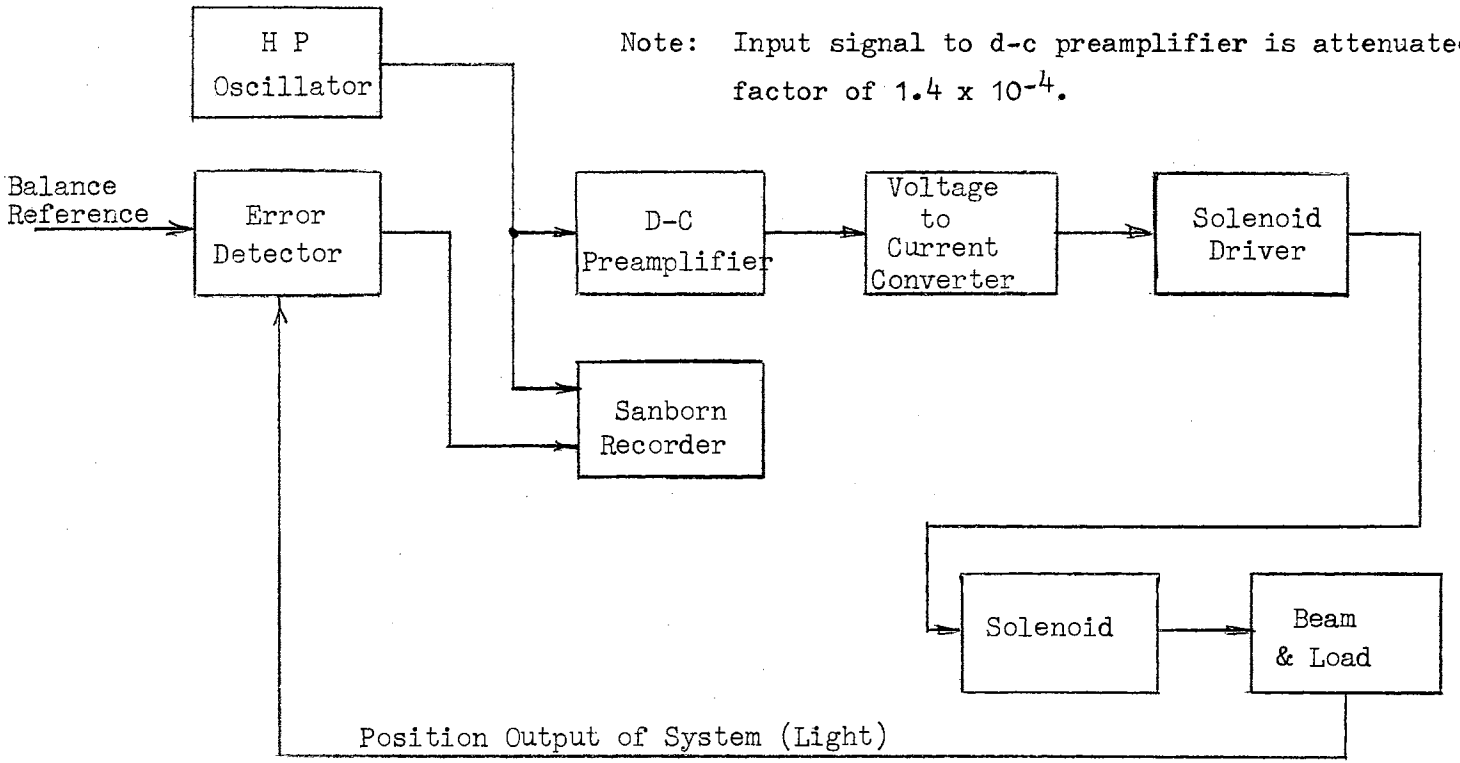

Figure 14. Testing Procedure for the Control System

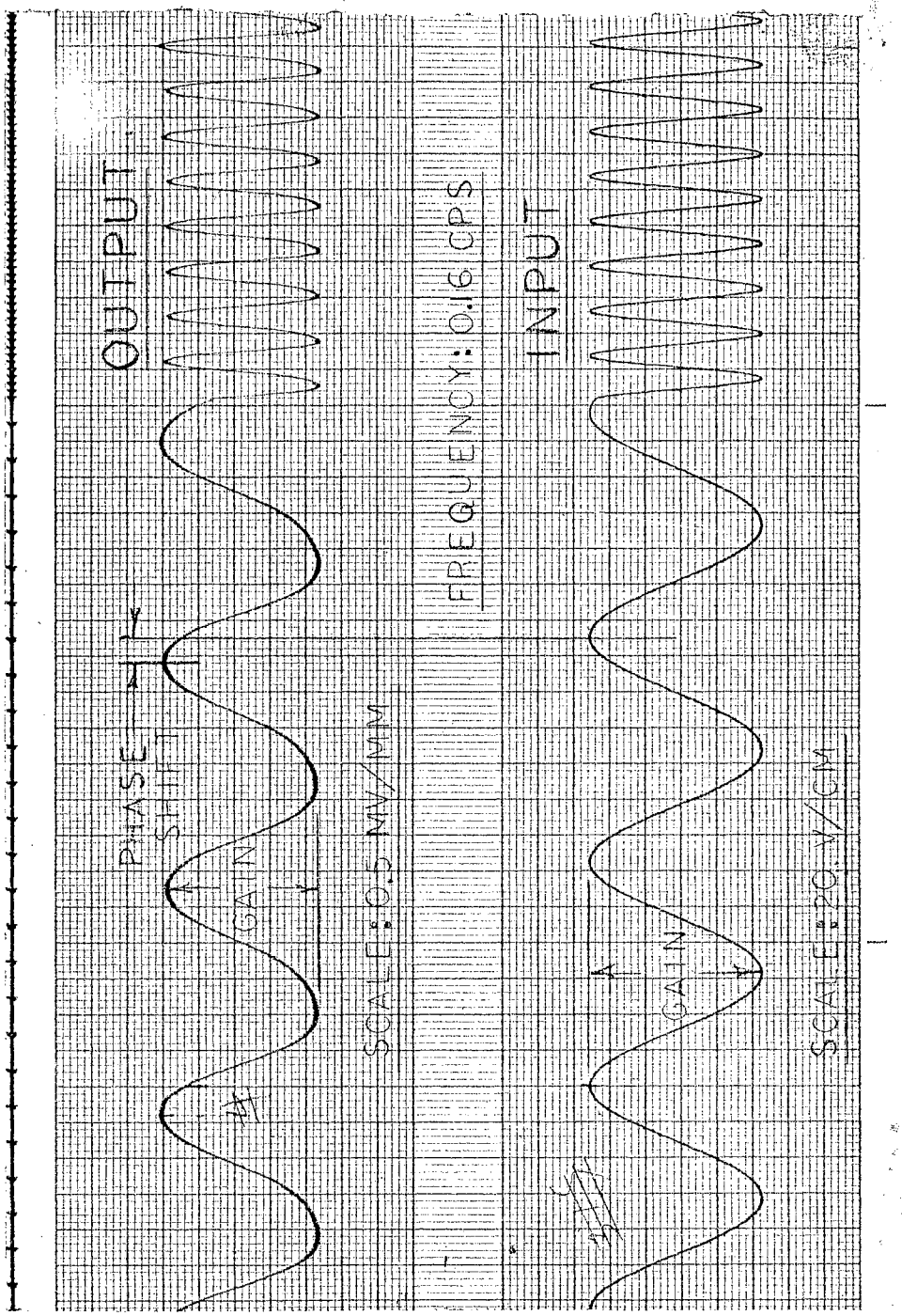

Figure 15. Example of Recorder Chart Paper

The information needed to construct the Bode diagram was extracted from the recorder chart and tabulated. Then the data was transferred to semi-log graph paper (two-cycle). The tabulation (Table II) gives for each frequency setting, the output level, the ratio $\left|\frac{E_o}{E_{in}}\right|$, the value of $20 \log \left|\frac{E_o}{E_{in}}\right|$, and the phase ϕ. The desired Bode diagram is shown in Figure 16.

Approximating the Transfer Characteristic

The open-loop transfer function of the system may be approximated by observing the gain magnitude and phase as obtained from the experimental data. Letting the transfer function be designated by G(s), then the approximate function is of the form

$$G(s) = \frac{K\,(1 + \tau_2 s)}{(1 + \tau_1 s)\,(1 + \tau_3 s)\,\left(\frac{1}{\omega_n^2} s^2 + \frac{2\zeta}{\omega_n} s + 1\right)} \qquad (1)$$

This function may be verified as a close approximation by substituting values for τ_1, τ_2, τ_3, ζ and ω_n and sketching a Bode plot of the results.

The value for the the factor ζ may be obtained from the Bode diagram. However, the term with break frequency $1/\tau_3$ distorts the peaking of the quadratic term and thus obscures the true peak.

From judicious inspection, the following values for the coefficients are chosen, $1/\tau_1 = 0.45$, $1/\tau_2 = 0.5$, $1/\tau_3 = 0.8$, $\zeta = 0.2$, $\omega_n = 1.5$, then equation (1), after some manipulation, becomes

TABLE II

Experimental Data on Uncompensated System

Frequency (rad/sec)	Output (mv)	$\left\lvert \frac{E_o}{E_{in}} \right\rvert$	20 log $\left\lvert \frac{E_o}{E_{in}} \right\rvert$	Phase (in degrees)
0.47	8.5	1.27	2.0	- 16.0
0.50	8.0	1.20	1.6	- 26.0
0.53	7.5	1.12	1.0	- 24.5
0.56	8.0	1.20	1.6	- 30.0
0.60	8.0	1.20	1.6	
0.63	8.0	1.20	1.6	
0.75	9.0	1.34	2.6	- 26.0
0.88	10.0	1.50	3.5	- 45.0
1.00	11.0	1.64	4.3	- 45.6
1.13	12.5	1.87	5.2	- 51.0
1.26	14.0	2.1	6.4	- 51.0
1.57	12.0	1.8	5.1	-210.0
1.88	7.0	1.05	0.4	-230.0
2.20	3.5	0.52	-0.3	-255.0
2.50	0.5	0.075	-1.125	-260.0

Input: 6.7×10^{-3} v = 6.7 mv

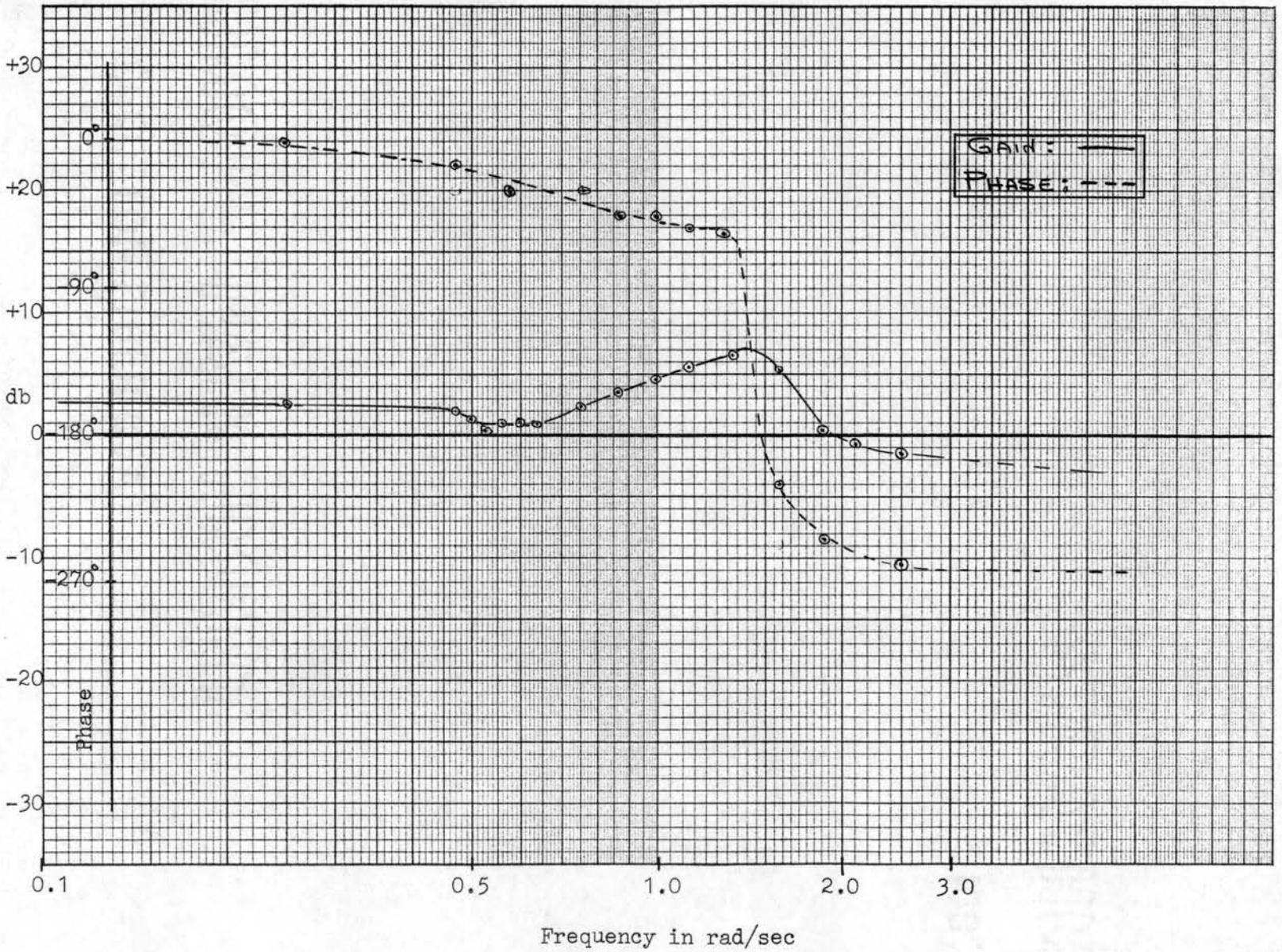

Figure 16. Bode Diagram of the Uncompensated System

$$G(s) = \frac{1.3\ (2.0s + 1)}{(2.2s + 1)\ (1.25s + 1)\ (s^2 + 0.6s + 2.25)} \quad (2)$$

The constant term in the numerator becomes

$$20 \log 1.6 = 4.0 \text{ db}$$

with 0° phase shift.

The zero at -0.5 plots along the 0 db line to the break frequency 0.5 radians per second, then proceeds positive with a 6 db/octave slope. The phase plot is contained between the boundary 0° and $+90^\circ$, crossing the point $+45^\circ$ at the break frequency, 0.5 rad/sec. The poles at -0.45 and -0.8 plot in the same general manner as the zero except the slope of the poles goes negative at the break frequencies. Also the phase begins at 0° and proceeds negative to -90°.

The quadratic term is a little more difficult to plot due to the damping factor ζ. For $\omega << \omega_n$ the gain magnitude is 0 db and for $\omega >> \omega_n$ the gain plots at a 12 db/octave negative slope. The intersection of the 0 db line and the -12 db/octave asymptote occurs at a frequency equal to ω_n or 1.4 rad/sec. However, the plot of the gain magnitude near the break frequency is greatly influenced by the damping factor ζ. Templates are normally used to plot the gain and phase near the corner frequency, ω_n.

Because the logarithm of the transfer function is the sum of the logarithms of the individual terms, a composite plot of G(s) may be easily obtained. This plot (Figure 17) compares favorably with the experimentally derived plot.

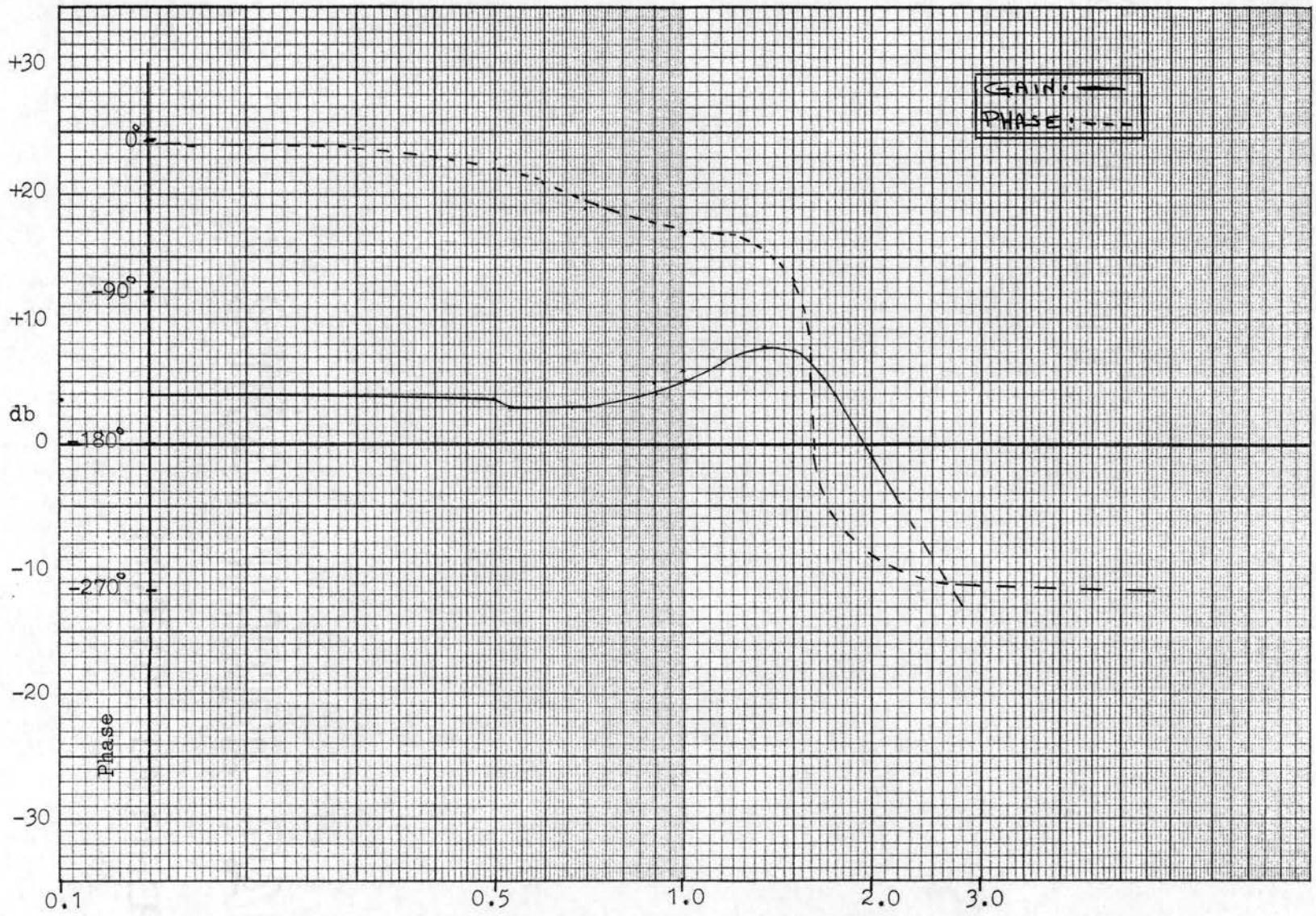

Figure 17. Bode Diagram of G(s)

Interpretation of the Results

The Bode plot of the transfer function G(s) revealed several important characteristics of the control systems. For one thing, it shows the system is a type zero system, since the approximate expression G(s) contains no integration terms (1/s). More important, the Bode plot shows the system to be unstable at frequencies greater than 0.15 cycles per second.

Referring to Figure 16, the peaking of the gain magnitude and the sharp downward trend of the phase at the frequency of 0.18 radian per second is interpreted as the natural frequency of the balance beam. As the driving frequency approached 0.18 radians per second, the undamped balance beam began to oscillate at an increasing amplitude.

The fact the Bode diagram indicated the system unstable requires that something be done to the system to insure stability of operation. The solution to the unstability problem would be to investigate the possibility of introducing some compensation to the system by means of a passive network. This would allow a minimum of modification to the existing system. So the first step to improvement of the system was to study the frequency response curve and determine what factor or combination of factors may be combined with G(s) to produce a stable system. Referring to Figure 16, it is obvious that by forcing the gain magnitude negative at the frequency 0.4 radians per second, the phase margin would be greatly improved and, in fact, stabilize the system. This type of compensation would be, in effect, a low-pass filter.

It was decided to add lag compensation into the system which would break downward at 12 db/oct at the corner frequency of 0.4 radian

per second . Consider the circuit in Figure 18. The transfer function,

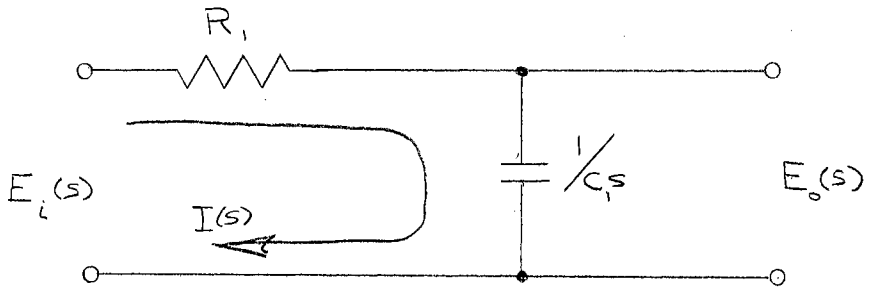

Figure 18

N(s), may be determined by circuit analysis techniques.

Then, assuming no load,

$$E_o(s) = \frac{I(s)}{C_1 s}$$

but

$$I(s) = \frac{E_i(s)}{R_1 + \frac{1}{C_1 s}}$$

Thus, the ratio of output to input becomes,

$$\frac{E_o(s)}{E_i(s)} = N(s) = \frac{\frac{1}{C_1 s}}{R_1 + \frac{1}{C_1 s}} \qquad (3)$$

which is the transfer function of the network. Rewriting equation (3) gives

$$N(s) = \frac{1}{R_1 C_1 s + 1} \qquad (4)$$

The Bode plot of the function represented by equation (4), however,

does not give the desired 12 db/octave asymptote. Rather, it breaks at 6 db/oct as may be shown by letting $\tau_4 \omega >> 1$, then

$$\begin{aligned} 20 \log \left| N(s) \right| &= -20 \log \left| \tau_4 (j\omega) + 1 \right| \\ &= -20 \log \left| \tau_4 \omega \right| \end{aligned} \tag{5}$$

where τ_4 is equal to $R_1 C_1$

Equation (5) plots as a straight line with -6 db/octave slope.

To the casual observer, it may appear that the solution is to combine two networks such as Figure 18. This would, indeed, produce the desired -12 db/octave slope. However, if the network consisting of two stages of Figure 18 were used, the resultant transfer function would not be of the desired form:

$$H(s) = \frac{1}{(\tau_4 s + 1)^2}$$

This is due primarily to the loading effect of the second section upon the first section. For, considering the network of Figure 19, the

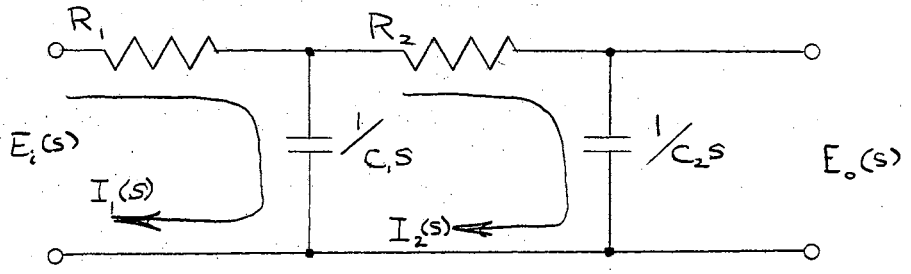

Figure 19. Cascaded Compensating Network

transfer function, called it H(s), may be determined by network analysis. Assuming currents I_1 and I_2 and no load on the output:

$$E_i(s) = R_1 I_1(s) + \frac{1}{C_1 s} I_1(s) - \frac{1}{C_1 s} I_2(s)$$

$$0 = -\frac{1}{C_1 s} I_1(s) + R_2 I_2(s) + \left(\frac{1}{C_1 s} + \frac{1}{C_2 s}\right) I_2(s) \tag{6}$$

Rewriting Equation (6),

$$E_i(s) = \left(R_1 + \frac{1}{C_1 s}\right) I_1(s) - \frac{1}{C_1 s} I_2(s)$$

$$0 = -\frac{1}{C_1 s} I_1(s) + \left[R_2 + \left(\frac{1}{C_1 s} + \frac{1}{C_2 s}\right)\right] I_2(s)$$

Solving for $I_2(s)$ by applying Cramer's rule gives

$$I_2(s) = \frac{\begin{vmatrix} R_1 + \frac{1}{C_1 s} & E_i(s) \\ -\frac{1}{C_1 s} & 0 \end{vmatrix}}{\begin{vmatrix} R_1 + \frac{1}{C_1 s} & -\frac{1}{C_1 s} \\ -\frac{1}{C_1 s} & R_2 + \frac{1}{C_1 s} + \frac{1}{C_2 s} \end{vmatrix}}$$

$$I_2(s) = \frac{E_i(s)}{R_1 R_2 C_1 s + (R_1 + R_2) + \frac{R_1 C_1}{C_2} + \frac{1}{C_2 s}} \tag{7}$$

But $I_2(s)$ may be expressed as:

$$E_o(s) = \frac{1}{C_2 s} I_2(s)$$

or

$$I_2(s) = C_2 s E_o(s) . \tag{8}$$

Substituting Equation (8) into Equation (7) yields

$$C_2 s E_o(s) = \frac{E_i(s)}{R_1 R_2 C_1 s + \left(R_1 + R_2 + \frac{R_1 C_1}{C_2} \right) + \frac{1}{C_2 s}}$$

Dividing through both sides by $C_2 s$ gives;

$$\frac{E_o(s)}{E_1(s)} = \frac{1}{R_1 R_2 C_1 C_2 s^2 + (R_1 C_2 + R_2 C_2 + R_1 C_1) s + 1}$$

Thus,

$$H(s) = \frac{1}{R_1 R_2 C_1 C_2 s^2 + \left[(C_1 + C_2) R_1 + R_2 C_2 \right] s + 1} \tag{9}$$

This is obviously not the transfer function which is needed to give the proper break in the gain magnitude curve. However, the transfer function H(s) may be made to approximate N(s) by an adjustment of the network component values. The desired transfer function is

$$N(s) = \frac{1}{(\tau_4 s + 1)^2} = \frac{1}{\tau_4^2 s^2 + 2\tau_4 s + 1} \tag{10}$$

where $\tau_4 = RC$.

Letting $R_2 = 10R_1$, and $C_2 = 1/10\ C_1$, then Equation (9) becomes

$$H(s) \approx \frac{1}{R_2^2 C_2^2 s^2 + 2R_2C_2s + 1} \tag{11}$$

By choosing $\tau_4 = R_2C_2$, Equation (11) becomes

$$H(s) \approx N(s) = \frac{1}{\tau_4^2 s^2 + 2\tau_4 s + 1} \tag{12}$$

It may be observed that τ_4 also equals R_1C_1 from the assumptions that $R_2 = 10R_1$ and $C_2 = 1/10\ C_1$.

This network with the values indicated in Figure 20 was then

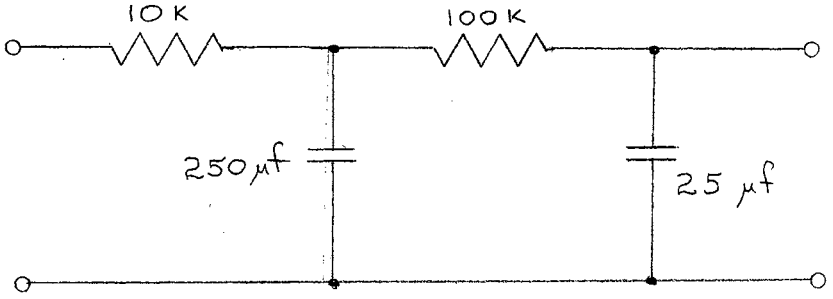

Break Frequency: 0.4 rad/sec

Figure 20. Network with Values Indicated

introduced into the control system to form what will be called the improved system. The transfer function for the improved system will take the form

$$G_c(s) = N(s)G(s)$$

$$G_c(s) = \frac{K\ (1 + \tau_2 s)}{(1 + \tau_1 s)\ (1 + \tau_3 s)\ (1 + \tau_4 s)^2 \left[\frac{1}{\omega_n^2} s^2 + \frac{2\zeta}{\omega_n} s + 1\right]} \tag{13}$$

Tests on the Improved System

The compensating network discussed in the preceding section was inserted into the microbalance control system between the d-c preamplifier and the voltage to current converter as shown in Figure 21. The compensating network was inserted at this point in the control loop to take advantage of the input/output characteristics of the neighboring units. This is important since loading of the compensating network would change its frequency response characteristics.

The same test was performed on the improved system as was on the uncompensated system. The resulting data was extracted from the recorder chart as before and tabulated. (See Table III). From this table the Bode diagram was drawn (Figure 22).

Interpretation of Results of Tests on the Improved System

As Figure 22 indicates, the compensation cascaded with the system caused the gain magnitude to decrease at the proper frequencies to assure stability. The phase margin is large enough with the added compensating network to also assure stability in closed-loop operation.

It would be of interest at this point to consider the improved system's steady-state performance. From Chapter II, it may be deduced that the open-loop is a type zero system. The transfer function is

$$\frac{\theta_c(s)}{E(s)} = G(s) = \frac{K\,(1 + \tau_2 s)}{(1 + \tau_1 s)(1 + \tau_3 s)(1 + \tau_4 s)^2\left(\frac{1}{\omega_n^2}s^2 + \frac{2\zeta}{\omega_n}s + 1\right)} \qquad (14)$$

For unity feedback, $\theta_c(s)$ is the output of the main control path and

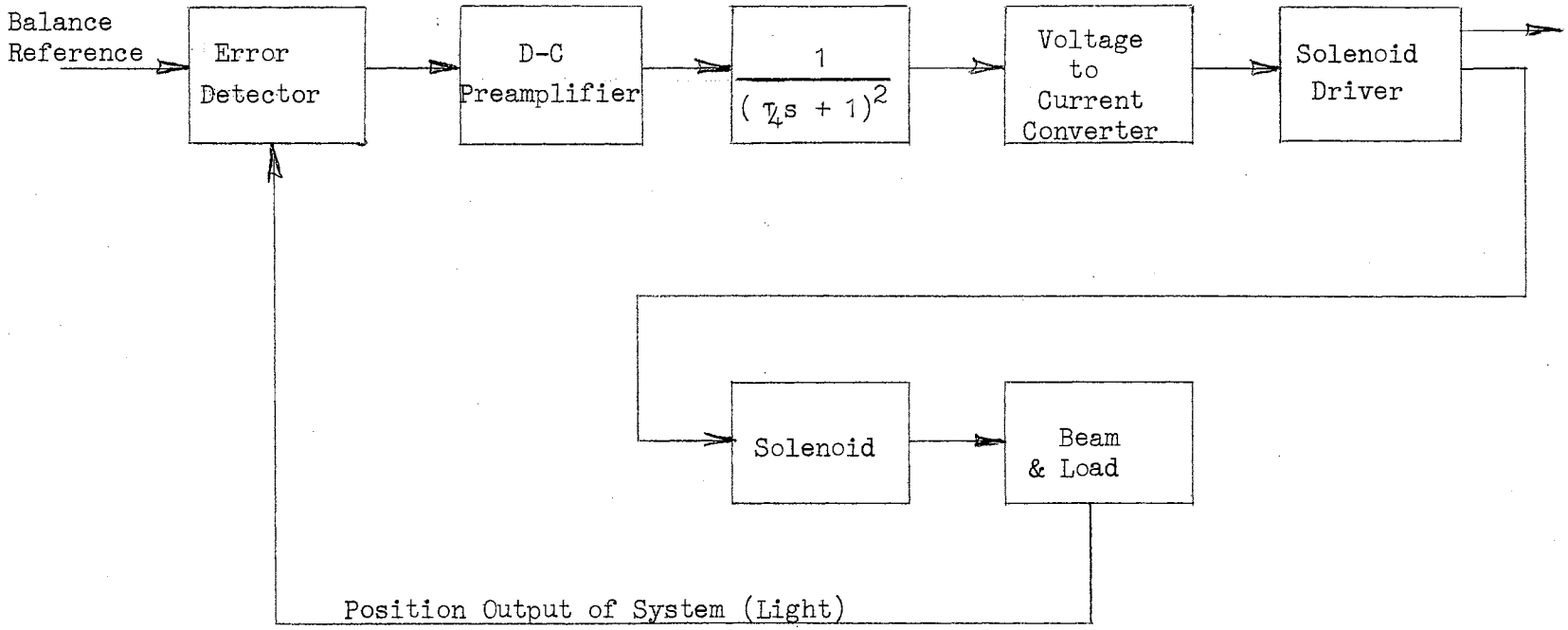

Figure 21. Control System with Compensating Network

TABLE III

Experimental Data on Improved System

Frequency (rad/sec)	Output (mv)	$\left\lvert \frac{E_o}{E_{in}} \right\rvert$	20 log $\left\lvert \frac{E_o}{E_{in}} \right\rvert$	Phase (in degrees)
.0628	15.0	2.15	6.6	- 28
.126	11.0	1.57	4.0	- 63
.188	9.5	1.29	2.2	- 76
.22	7.5	1.07	1.6	-105
.25	7.0	1.00	0.0	-102
.35	6.0	.86	-1.5	-100
.375	5.5	.78	-2.4	- 98
.44	4.0	.57	-5.0	-105
.51	5.0	.71	-3.0	-126
.56	3.5	.50	-6.0	-126
.628	.4	.057	-25.0	-175
.93	.45	.065	-23.8	-180
1.26	.5	.071	-23.0	-270

Input: 6.7×10^{-3} volts.

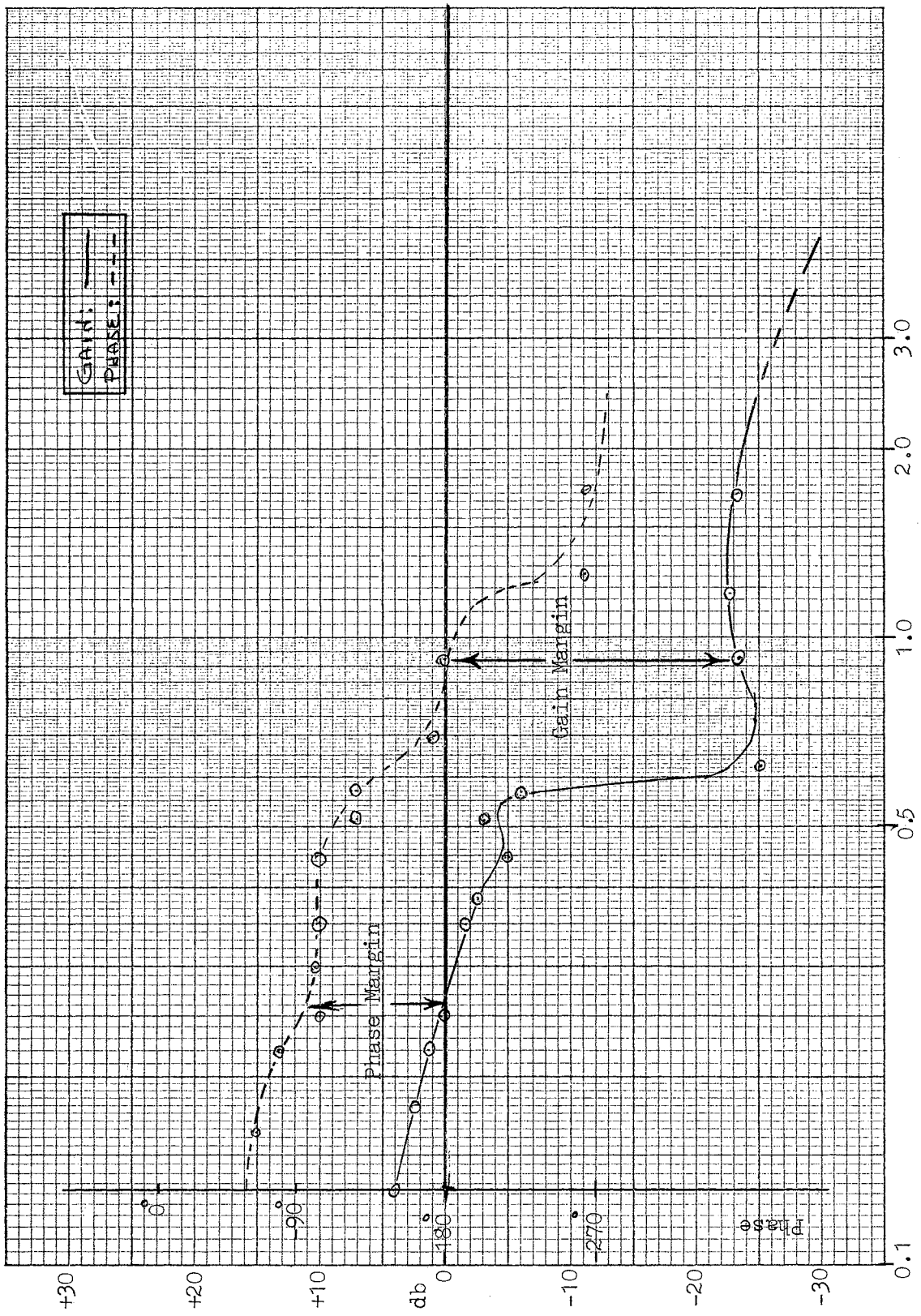

Figure 22. Bode Diagram of the Compensated System

E(s) is the signal from the error detector. Since the system under study has unity feedback, the block diagram of the closed-loop system is as shown in Figure 23.

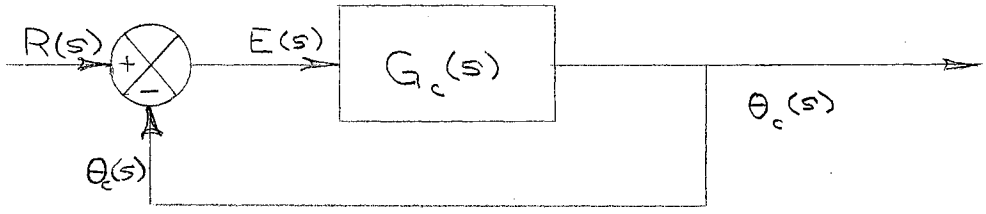

Figure 23. Closed-loop Block Diagram

The closed-loop transfer function would then be

$$\frac{R(s)}{\theta_c(s)} = \frac{1}{1 + G_c(s)} \tag{15}$$

To establish the steady-state performance of the system, the first characteristic to be checked is the steady state error. The position constant, K_p, is defined as

$$K_p = \lim_{s \to o} G(s) \tag{16}$$

To determine the steady state error of a type zero unity feedback system, a relationship must be established between the input to the system, R(s), and the closed-loop transform. This involves a so-called error series which will not be discussed since only the results are of importance at this point. Appendix B contains the results of this series. Referring to the Table II in Appendix B, it may be observed that a step-function input is the only permissible input since higher order functions would yield an increasing steady state error. Fortunately, in the microbalance system, R(s) is a step-function input,

so the system steady-state error is given by

$$E_{ss}(s) = \frac{1}{1 + K_p} \cdot \text{Input Volts} \tag{17}$$

Note that for a large position constant, K_p, the error E_{ss} is small.

From Equation (16) the position constant for this system is

$$K_p = \lim_{s \to o} G(s) = 1.5$$

So, from Equation (17), the steady-state error is

$$E_{ss}(s) = \frac{1}{1 + 1.5} = 0.4 \cdot \text{Input Volts}$$

CHAPTER VI

DISCUSSION OF THE RESULTS

Summary and Conclusions

The investigation of the microbalance control system was embarked upon to determine mainly three characteristics: the system stability, the margin of stability, and the steady-state error. After experimental data were collected from the system and assembled in a fashion conducive to examination, the writer found the control system unstable. From the information obtained from the experimental data, however, a good approximation of the system transfer function equation was obtained. This allowed the writer to investigate the possibility of improvement of the system through compensation. An improved system was devised by cascading the system control loop with a compensation network. Tests were then performed to verify the proposed stabilizing of the system thorugh passive network compensation. The results of the tests revealed that the improved system was indeed stable and with a considerable stability margin. With stability achieved, the gain and phase margins were obtained, along with the steady-state error characteristics.

The steady-state error of this system offers some concern, since it is a function of the gain, K, of the system. To minimize the steady-state error, a large position constant K_p is required as shown by the equation,

$$E_{ss}(s) = \frac{1}{1 + K_p} \qquad (1)$$

The first solution which comes to mind is to increase the gain of the forward loop. However, the stability of the control loop is a function of the gain and if the gain were increased beyond the gain margin, which has been established, the system would become unstable. Thus, a compromise must be made between sensitivity of the balance and stability.

The possibility exists that the system could be further modified to achieve zero steady state error. For instance, if the system could be changed to a type one system, then, referring to Table II of Appendix B, the closed-loop system would have a zero steady-state error with a step-function input. This would be highly desirable for a precision measuring instrument such as the microbalance.

Suggestions for Future Study

The basic objective of future investigation of this control system would undoubtedly be launched in an effort to improve the automatic control of the microbalance. Therefore, the possibility of achieving a steady-state error of zero would definitely be investigated. A component which will insert a pole at the origin of the root-locus plot should be explored as a possible method of modifying the system to a type one.

The nonlinearities in the control system components did not hamper operation of the balance in the course of this investigation. However, nonlinearities do exist since, for example, the solenoid driver is somewhat a nonlinear device. The effect of these nonlinear components on system performance could be investigated and improvements noted.

The effects of the nonlinearities in the control system components were not serious for the normal operating range of signal magnitude and frequency.

A SELECTED BIBLIOGRAPHY

Ahrendt, W. R. and C. J. Savant. Servomechanism Practice. New York: McGraw-Hill, 1960.

Ahrendt, W. R. and J. F. Taplin. Automatic Feedback Control. New York: McGraw-Hill, 1951.

Behrndt, K. H., ed. Vacuum Microbalance Techniques, Vol. 3. New York: Plenum Press, Inc., 1963.

Brown, G. S., and D. P. Campbell. Principles of Servomechanisms. New York: John Wiley and Sones, Inc., 1948.

Bruns, R. A. and R. M. Saunders. Analysis of Feedback Control Systems. New York: McGraw-Hill, 1955.

Cahn, L. and H. R. Schultz. Vacuum Microbalance Techniques, Vol. 2., 1962, p. 7.

Cochran, C. N. Vacuum Microbalance Techniques, Vol. 1., 1961, p. 23.

Czanderna, A. W. and J. M. Honig. Analytical Chemistry, Vol. 29, 1957, p. 1206.

Emich, F. Abderhalden, Vol. 9, 1919. p. 55.

Emich, F. Lehrbuch der Mikrochemie. Munich: Bergman and Co., 1926.

Gorbach, G. Mikrochemie, Vol. 15, 1936, p. 254.

Gruber, J. L. and C. S. Shipley. Vacuum Microbalance Techniques, Vol. 1, 1961, p. 23.

Hazen, H. L. Theory of Servomechanisms. New York: J. Franklin Institute, 1934.

Ingram, G. Metallurgia, Vol. 39, 1949, p. 232.

Katz, M. J., ed. Vacuum Microbalance Techniques, Vol. 1. New York: Plenum Press, Inc., 1961.

Kirk, P. L. Quantitative Ultra-Microanalysis. New York: John Wiley & Sons, 1942.

Lago, Gladwyn and L. M. Benningfield. Control System Theory. New York:

Mayer, H. et al., Vacuum Microbalance Techniques, Vol. 3, 1963, p. 75.

Pearson, E. B. Technology of Instrumentation. London: The English Universities Press, Ltd., 1957.

Pettersson, H. Proc. Phys. Soc., Vol. 32. (London), 1920, p. 209.

Raven, F. H. Automatic Control Engineering. New York: McGraw-Hill, 1961.

Salvioni, E. Dissertation, University of Messina, 1901.

Steele, B. D. and K. Grant. Proc. Roy. Soc., Vol. A82 (London), 1909, p. 580.

Strom, H. F. Magnetic Amplifiers. New York: John Wiley and Sons, Inc., 1955.

Thaler, G. J. and R. G. Brown. Analysis and Design of Feedback Control Systems. New York: McGraw-Hill, 1960.

Truxal, J. G. Control Engineers Handbook. New York: McGraw-Hill, 1951.

Truxal, J. G. Control System Synthesis. New York: McGraw-Hill, 1955.

Walker, R. F., ed. Vacuum Microbalance Techniques, Vol. 2. New York: Plenum Press, Inc., 1962.

APPENDIX A

Useful LaPlace Transform Pairs

f(t)	F(s)
u(t) [step function]	$1/s$
$u_1(t)$ [impulse function]	1
ϵ^{-at}	$1/s + a$
ϵ^{at}	$1/s - a$
$\sin \omega t$	$\omega/s^2 + \omega^2$
$\cos \omega t$	$s/s^2 + \omega^2$
$t^n/n!$	$1/s^{n+1}$
$\int_0^t f(t)dt$	$1/s\ F(s)$
$f'(t)$	$sF(s) - f(0)$
$f''(t)$	$s^2F(s) - sf(0) - f'(0)$
$f'''(t)$	$s^3F(s) - s^2f(0) - sf'f(0) - f''(0)$

APPENDIX B

Given that G(s) = open-loop transfer function, then the static error coefficients are

Position Constant:

$$K_p = \lim_{s \to 0} G(s)$$

Velocity Constant:

$$K_v = \lim_{s \to 0} sG(s)$$

Acceleration Constant:

$$K_a = \lim_{s \to 0} s^2G(s)$$

Table I shows the relationship between static error coefficients and the system type numbers.

Table II shows the steady-state error for different inputs and system types.

Table I

TYPE	0	1	2
K_p	K_p (finite)	∞	∞
K_v	0	K_v (finite)	∞
K_a	0	0	K_a (finite)

Table II

	Input		
Type	$u_{-1}(t)$	$u_{-2}(t)$	$u_{-3}(t)$
0	$\frac{1}{1 + K_p}$	∞	∞
1	0	$\frac{1}{K_v}$	∞
2	0	0	$\frac{1}{K_a}$

APPENDIX C

In the construction of a transfer function, one need only consider four basic types of factors. These are:

$$K \text{ (constant)} \qquad (1)$$

$$|j\omega|^n \qquad (2)$$

$$|j\omega + 1|^n \qquad (3)$$

$$|(j\omega)^2 a + j\omega b + 1| \qquad (4)$$

For example, a very common function in positioning servomechanisms is one of the form:

$$|G(j\omega)| = \frac{1}{|j\omega|\,|j\omega\tau_1 + 1|\,|j\omega\tau_2 + 1|} \qquad (5)$$

In this case, $G(j\omega)$ contains (1), (2) with $n = -1$, (3) with $n = -1$. The plot of $20 \log|G(j\omega)|$ against $\log \omega$ may be easily obtained by considering each factor separately and then forming a composite graph.

K(Constant)

The factor K is generally a gain factor and is not a function of frequency. Thus, $20 \log|K|$ is invarient with $\log \omega$ and plots as a horizontal line. The phase angle is 0° for all ω.

$|j\omega|^n$

This factor may be in the numerator or the denominator of the transfer function. If it is in the numerator, the number n is positive,

which yields

$$20 \log \left| j\omega \right|^n = n\ 20 \log \left| j\omega \right| \tag{6}$$

The slope will then be positive with increasing ω and the phase angle will be $n \cdot 90^\circ$.

If the factor is in the denominator, the log becomes

$$20 \log \left| j\omega \right|^{-n} = -n\ 20 \log \left| j\omega \right| \tag{7}$$

The slope will be negative with increasing ω and the phase angle will be $-n \cdot 90^\circ$.

The number n also determines the magnitude of the slope in addition to the sign. If n = 1, the slope is 6db/octave, n = 2, the slope is 12db/octave, et cetera.

$$\left| \omega\tau + 1 \right|^n$$

This factor may also be in either the numerator or the denominator of a given function. Also the number n determines the steepness of the slope in db/octave.

To obtain a plot of this function, the asymptotic approximation is generally utilized. If we observe that for values of $\omega\tau << 1$, 20 log $\left| j\omega\tau + 1 \right|^n$ evaluates to 0 db. Also, for values of $\omega\tau >> 1$, 20 log $\left| j\omega\tau + 1 \right|^n$ reduces to (20) (n) log $\left| j\omega \right|$. At $\omega\tau = 1$, the equation becomes

$$20 \log \left| 1 + 1 \right|^n = 20\ n \log \left| 2 \right| = 3.02\ n \tag{8}$$

This point $\omega\tau = 1$ or $\omega = 1/\tau$ is called the corner frequency or 3 db point.

The phase (ϕ) of $\left| j\omega\tau + 1 \right|^n$ is given by

$$\phi = \tan^{-1} \left| \omega\tau \right| \qquad (9)$$

$$\left| (j\omega)^2 a + (j\omega)b + 1 \right|$$

The log of this factor is also expressable in terms of asymptotes. For $\omega << 1$, 20 log $\left|(j\omega)^2 a + j\omega b + 1\right|$ evaluates to 0 db. At high frequencies, the term $a(j\omega)^2$ dominates and the factor becomes

$$20 \log \left| a(j\omega) \right|^2 = -40 \log \left| \sqrt{a}\, \omega \right| \qquad (10)$$

This results in a 12 db-octave slope.

The asymptotes intersect at the 0 db axis at the frequency $\omega = 1/\sqrt{a}$. Of course the true magnitude of the curve is a function of the damping ratio and thus depends on the coefficient b. Generally, the approximation using asymptotes is accurate enough.

Corrections can be made from a master template[1] which is made up of a family of curves depending on the damping factor. A plot of the four factors is given in Figure 1.

---

[1] Thaler and Brown, Analysis and Design of Feedback Control Systems, p. 158.

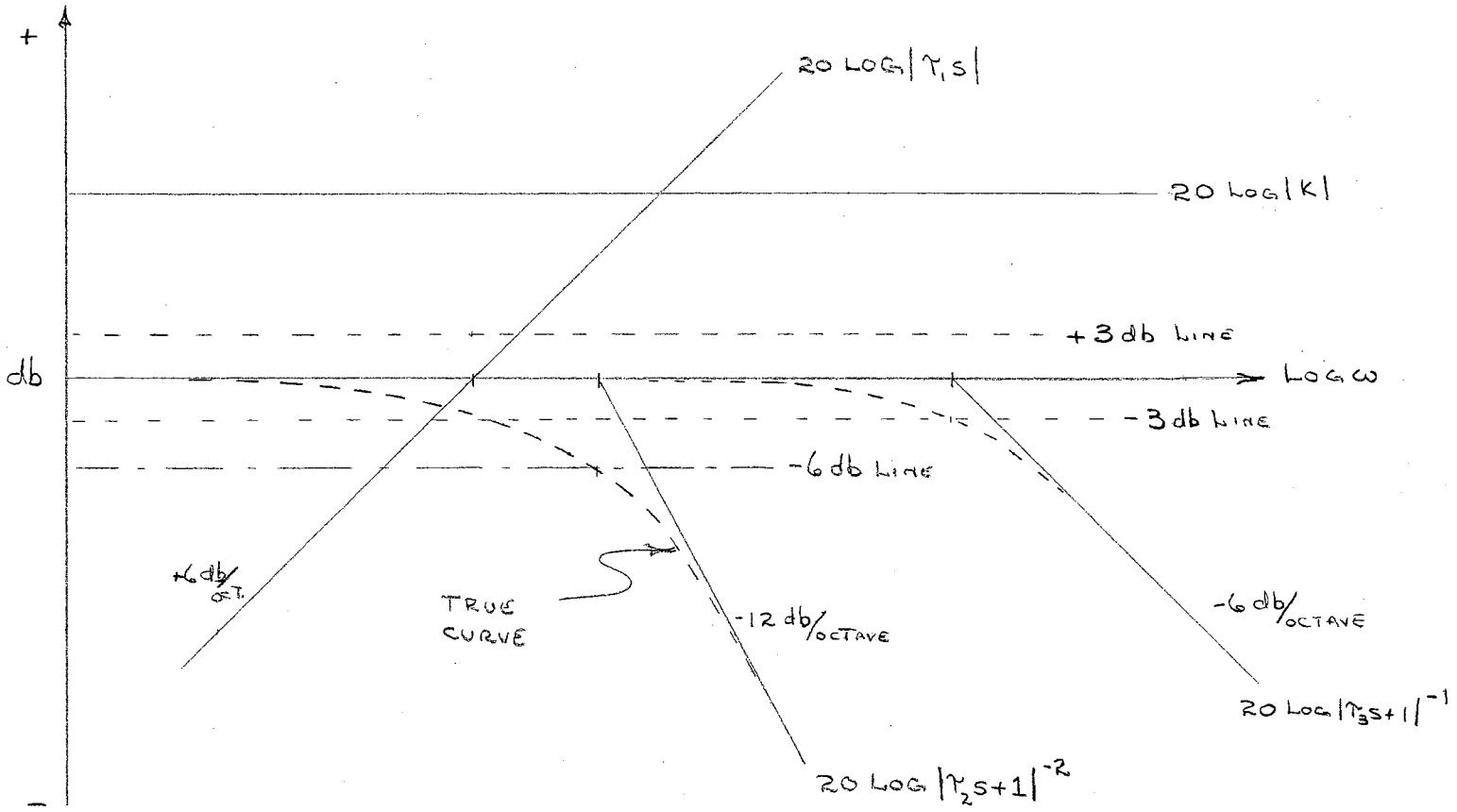

Figure 1. Plot of Logarithm of Various Factors Versus log ω.

VITA

Harvard Lynn Tomlinson

Candidate for the Degree of

Master of Science

Thesis: A SERVO CONTROLLED DYNAMIC LOAD MICROBALANCE

Major Field: Electrical Engineering

Biographical:

Personal Data: Born at Duncan, Oklahoma, March 31, 1937, the son of Harvard B. and Vera Maxine Tomlinson.

Education: Attended high school at Cushing and Stillwater, Oklahoma; graduated from Stillwater High School in May, 1954; received the Bachelor of Science degree from the Oklahoma State University, with a major in electrical engineering, in May, 1963; completed requirements for Master of Science, with a major in electrical engineering in August, 1964.

Professional experience: Entered the United States Navy Electronic Technician Class "A" School in 1956 and upon graduation was assigned shipboard electronic repair and maintenance duties until May, 1959; upon entering Oklahoma State University in the summer, 1959, held position of electronic technician with Dr. H. L. Jones, EE Dept, performing tasks in connection with the O.S.U. atmospheric research program; from May, 1962, functioned as electronic technician and later engineer for Dr. R. D. Freeman, Chemistry Dept., director of various physical chemistry research programs.